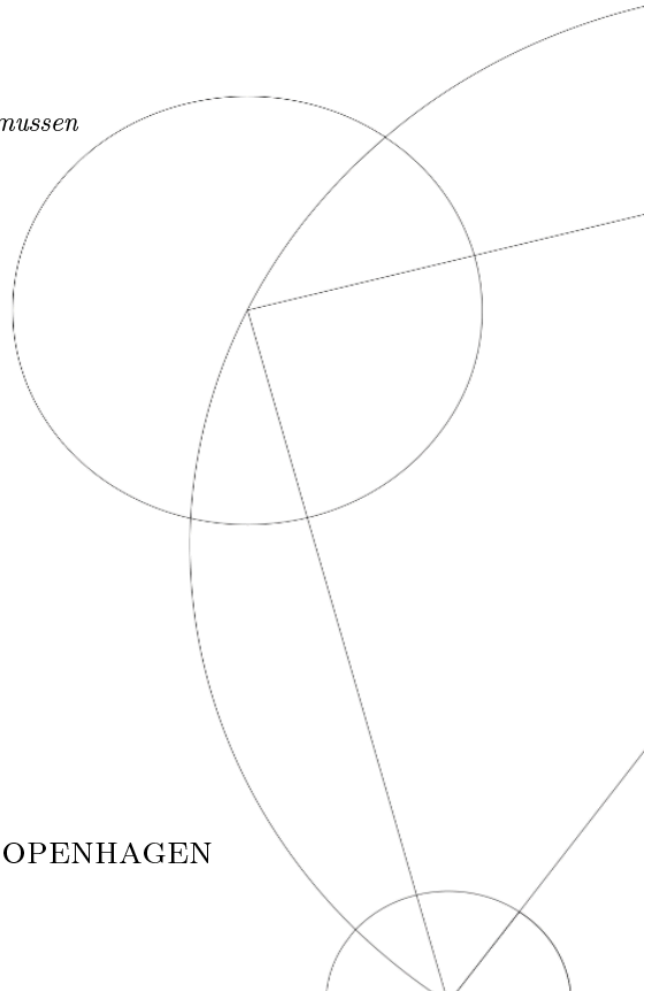# Electrostatic simulations of small arrays of Coulomb islands

Written by *Bertram Brovang and Torbjørn Raasø Rasmussen*
June 12, 2019


Supervised by
Ferdinand Kuemmeth

# University of Copenhagen

NAME OF INSTITUTE:    Niels Bohr Institute

NAME OF DEPARTMENT:   Center for Quantum Devices

AUTHOR(S):            Bertram Brovang and Torbjørn Raasø Rasmussen


TITLE AND SUBTITLE:   Electrostatic simulations of small
                      arrays of Coulomb islands
                      -

SUPERVISOR(S):        Ferdinand Kuemmeth

HANDED IN:            12.06.2019

# 0    Abstract

In this project we have simulated the electrostatic energy of a two by two quantum dot array, including the effects of tunneling between dots. In this project we have simulated charge stability diagrams for double and triple quantum dots. We have considered how the state of these double and triple quantum dots can be manipulated by application of time-dependent gate voltages, which can be visualised as trajectories in the gate-voltage space associated with the charge stability diagrams. Furthermore we have considered the shape of the three dimensional charge configurations, in the three dimensional charge stability diagram. Building upon these considerations we have done two-dimensional non-native-gate measurements of three-dimensional gate space and can propose a method of exchanging electrons in a triple quantum dot in a two by two quantum dot setup. Finally we have experimented with electron transport in a double dot, utilising specific trajectories in gate voltage space to pump electrons through the double dot.

# Contents

# 1 Introduction

The calculation power of computers have been exponentially increasing the last few decades and has opened up new fields such as machine learning and artificial intelligence. Technological advancements has allowed us to make transistors smaller and smaller to enable us to fit more and more transistors onto the same area. These advancements have also opened up for the manufacturing of new exciting devices to be used in spin qubits that could be used in a future computer that is based on principles from quantum mechanics. Computers like these have a potential to be many times more powerful than the computers of today and could lead to new research fields where computing power is essential. Operation of spin qubits in arrays of quantum dots will require precise control of electron charges within these arrays, which is the topic of this thesis. In our Bachelor project we have decided to create a simulation of electrostatically defined quantum dots in a small two-dimensional array of Coulomb islands. This constitutes a first step towards understanding and navigating in future, larger arrays. Furthermore, we believe there are many uses for a simulation of these types of systems such as in furthering machine learning for helping with the tuning of quantum dot setups.

# 2   Theory of quantum dots

Quantum dots are nanostructures that electrostatically define a region where it is possible to trap electrons, such that their energy levels are measureable [1]. Typically this is done by confining a 2-dimensional electron gas between conductors. In addition to kinetic effects (discrete quantum states due to size confinement), there is an electrostatic energy associated with quantum dots, which is typically larger than the discrete level spacing and the focus of this thesis.

## 2.1   Electrostatic Energy of Quantum dots

To calculate the electrostatic energy of the quantum dots in our simulation, we consider the capacitors in a system of many conductors. In actual devices we have many conductors influencing each dot, for our simulation we have two types of capacitive couplings. There is a capacitive coupling between each dot and each of the 8 gates, $c_{ij}$, and there is a capacitive coupling between each of the dots and all the other dots $c_{ik}$, with i being the index of the dot and j the index of the gate, while k is the index of the other dots, with $i = 1...4$ and $k = 01...04$ dots and $j = 1$ to $j = 8$ gates. In figure 1a there is a schematic representation of the dot to dot capacitances, and figure 1b shows a schematic representation of the capacitors between dots and the 4 plunger gates.
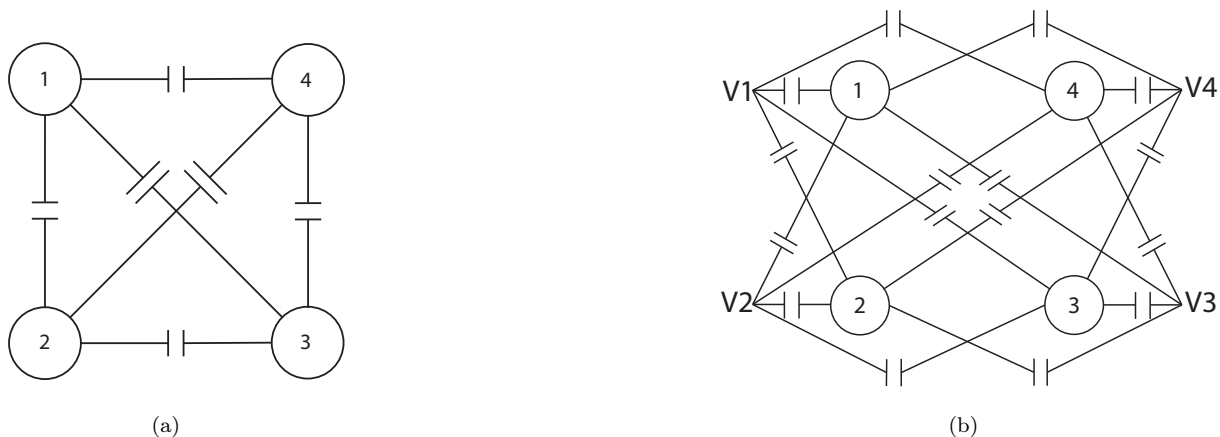


Figure 1: Array of Quantum dots (a) dot-to-dot capacitances, and (b) dot-to-gate capacitances of the 4 plunger gates.

The strongest of these capacitive couplings, is the coupling between a dot and the gates (see Sec. 2.2.1). With the coupling with its own plunger gate being the stronger and the coupling between a dot and one of the other dots plunger gate the weaker. The weakest coupling is the one between a dot and another dot.

$$c_{ii} > c_{ij} > c_{ik} \tag{1}$$

Each of these capacitors stores a charge and the total charge on one of the quantum dots is the total stored charge on the capacitors connected to it.

$$Q_i = \sum_{n=0}^{N} c_{in}(V_i - V_n) \tag{2}$$

Where $V_n$ is the potential of the $n'th$ node, nodes referring to *dots and gates*, the ground potential, $V_{n=0}$, defined as 0 and N being the total number of nodes in the system. The charge on a capacitor depends on the potential over it. The charge, quantized by $Q = -N_e \cdot e$, on the dots can thus be expressed as a linear function of this potential, here in matrix form.

$$\vec{Q} = \mathbf{C}\vec{V} \tag{3}$$

The diagonal elements of the matrix C is the total capacitance on dot i

$$C_{ii} = \sum_{n=0}^{N} c_{in}, \tag{4}$$

where N is the total number of nodes in the system. The off-diagonal elements is minus the capacitance between dot i and dot k, $C_{ik} = -c_{ik}$.

The electrostatic energy of the entire system can now be expressed using the charge vector defined in equation 3.

$$U = \frac{1}{2}\vec{V} \cdot \vec{Q} = \frac{1}{2}\vec{Q} \cdot \mathbf{C}^{-1}\vec{Q} \tag{5}$$

Since we know the voltages on the various gates, we only need to determine the voltages on the dots. We can write equation 3 as:

$$\begin{pmatrix} \vec{Q}_c \\ \vec{Q}_v \end{pmatrix} = \begin{pmatrix} \mathbf{C}_{cc} & \mathbf{C}_{cv} \\ \mathbf{C}_{vc} & \mathbf{C}_{vv} \end{pmatrix} \begin{pmatrix} \vec{V}_c \\ \vec{V}_v \end{pmatrix} \tag{6}$$

and then only focus on determining the voltages on dots, $\vec{V}_c$, by using:

$$\vec{V}_c = \mathbf{C}_{cc}^{-1}(\vec{Q}_c - \mathbf{C}_{cv}\vec{V}_v), \tag{7}$$

where the subscripts $v, c$ refer to voltage sources and dots. We can then calculate the total electrostatic energy using equation 5. [4]

In our simulation we sweep the voltage sources and, at each point in gate space, calculate the total electrostatic energy $U$ as a function of different charge configurations. In the case of $D$ dots and $N_e$ maximum electrons per dot, there will be a total of $(N_e + 1)^D$ configurations for the system to be in. We can then determine the minimum energy and the corresponding charge configuration which carries the lowest energy. This charge configuration will be the favorable configuration for the system to be in.

This is the basis of our simulation, and the various types of simulated measurements are based on this. From our simulation we can see that the energy of the different states takes the shape of parabolas, which arise from a quadratic dependence on voltage. This can be seen in figure 2 where the electrostatic energy of a double dot with 2 electrons per dot and 2 dots, is plotted as a function of gate voltage.
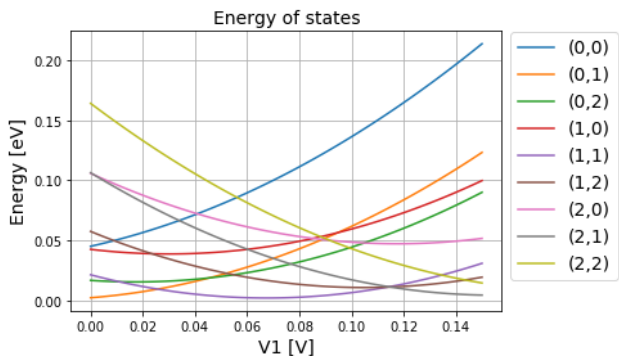


Figure 2: Energy functions of a double quantum dot with maximum 2 electrons per dot, here sweeping gate 1 and gate 2 set to 0.1V

## 2.2 Charge Stability Diagrams

The charge stability diagram of a device is of great practical importance. It is from the charge stability diagram we can interpret how our device behaves and how we can manipulate the electrons in the device. Figure 3 show the charge stability diagram for a double dot. The x-axis and y-axis respectively represents the voltage on gate one and gate two. The diagram illustrates the charge state for the ground state of the double dot for the different values of voltage on gate one and two, using color codes. The colors on the colorbar denote a state. The first index is the number of electrons on dot 1 and the second index is the number of electrons on dot 2, $(N_{e,dot1}, N_{e,dot2}, ..., N_{e,dotn})$. When working with actual devices we will not be measuring the actual charge state. Rather, we measure an indirect effect of the electrons movement in the quantum dots, such as current or impedance change. Although we are not measuring the charge state, as in our simulation,

we will however be seeing a very similar diagram. The diamond shapes that appear is common for all the different measurement types.

The shape and size of the diamond shapes can tell us a lot about our device and what its physical parameters are. If we consider the height of the diamond, this tells us how much the voltage has to increase or decrease to either add an electron to the dot or to repel an electron from the dot. Also, this tells us how much the dot is capacitively coupled to its gate since charge voltage, $\Delta V_C$, and capacitance, C, are related as:

$$\Delta V_C = \frac{e}{C} \tag{8}$$

The same logic follows on the width of the diamond. The slope of the diamonds edges tells us about the cross capacitance coupling. If we are at point near the top of a diamond in voltage space and we only



Figure 3: Charge stability diagram of double dot

increase the voltage on gate 1 we can see from the diagram that we move into a diamond which has an extra electron in dot 2. This tells us that dot 2 can feel the gate on dot 1 and reacts to the voltage on it. We can thus expect that the slope of the edges has to be negative if there is cross coupling. If there is no cross coupling then the edges would have to be horizontal and vertical, since it would be impossible to increase the number of electrons in dot 2 by increasing the voltage on gate 1.

The blue, green and yellow lines have been added to the charge stability diagram, to show the three different types of borders, that repeat throughout the diagram. Crossing a blue or green border will move an electron between the dots and the reservoirs, thereby increasing or decreasing the total number of electrons in the double dot. Crossing the yellow border will move an electron from one dot to the other, keeping the total number of electrons constant. The number of neighbours a state has, is a direct result of how many ways a given state can change by moving one electron. From figure 3 it can be seen that the states have six neighbouring states. Two of the neighbouring states have either had an electron move from dot 1 to dot 2, or from dot 2 to dot 1. These are called interdot transitions and happen when crossing a yellow border. When crossing a blue border, dot 2 will either gain or lose an electron. These two neighbouring states are above and below a state in the 2-dimensional gate-space. The last two neighbouring states are the states that either have one more electron or one less electron on dot 1. Transitioning to these states can be done by crossing the green border.

### 2.2.1 Extracting capacitances from charge stability diagrams

For the simulation to produce real looking data, we need to be able to input capacitances close to that of a real device. The charge stability diagram is the premier way of evaluating capacitances for an unknown device. We have already established the relation between charging voltage and capacitive coupling in equation 8 which we then use on charge stability diagrams to obtain realistic capacitances. The slope also tells us about the magnitude of the cross capacitance. For small interdot capacitances a negative slope of 20% on the gate 1 slope (green in figure 3) means that the cross capacitance between dot 1 and gate 2 is 20% of the capacitance between dot 1 and gate 1. In figure 4 we show an example
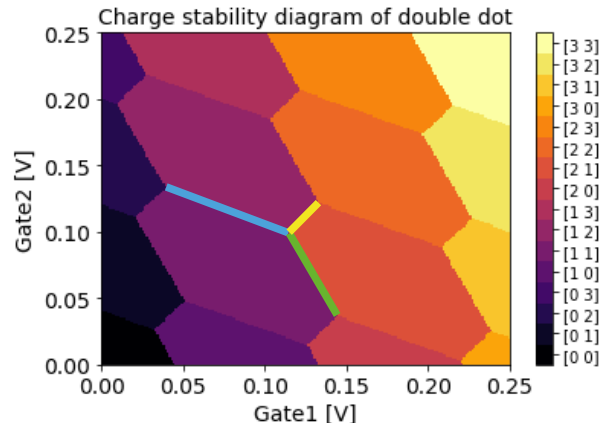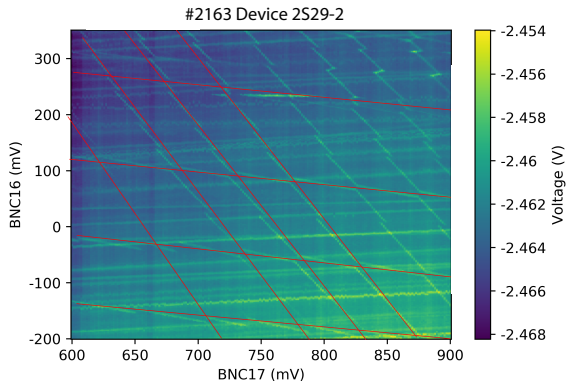


Figure 4: Measured charge stability diagram of real device

4

of a charge stability diagram used in this process with the red lines inserted for guidance. The dot to dot capacitances, are approximated using the formula for a plate capacitor, where the area A and distance d is approximated.

$$C = \epsilon_0 \epsilon \frac{A}{d} \tag{9}$$

The effectiveness of these methods can be questioned and we will revert to this in our discussion.

The result of the extraction process was a dot to gate capacitance matrix corresponding to the values represented by $c_{ii}$ and $c_{ij}$ in 1

$$c = \begin{pmatrix} 1.73 & 0.635 & 0.24 & 0.66 & 0 & 0 & 0 & 0 \\ 0.435 & 1.91 & 0.27 & X & 0 & 0 & 0 & 0 \\ 0.38 & 0.20 & 2.63 & X & 0 & 0 & 0 & 0 \\ 0.168 & X & X & 1.4 & 0 & 0 & 0 & 0 \end{pmatrix} \tag{10}$$

Here an X represents a dot to gate capacitance which we could not extract as we did not find suiting measurements. The found capacitances are all in aF. It can also be seen that the last four columns are empty, these are for future implementation of 4 more gates: source, drain, top and bottom. The dot to dot capacitance is estimated to be between 0.075aF and 0.105aF depending on the arrangement of the dots. We only use the capacitances of the active dots for each measurement. For dot 1 where we have extracted all capacitances, we estimate a typical charging energy of $50meV$.

## 2.3 Tunneling effects

Electrostatics do not provide the complete image. Our simulation also contains two tunneling effects, an interdot and a reservoir tunneling effect. The interdot tunneling effect is when an electron tunnels from one dot to another. An example of this would be (1000) to (0100), the electron from dot 1 tunnels to dot 2. The reservoir tunneling effect is when a dot gains an electron from the reservoir, either from the source or the drain. An example of this would be the states (1112) and (2112). Here dot 1 gained an electron, and the other three dots kept their electrons. In our simulation we only consider tunneling events with one electron.

To introduce the tunneling effects into our simulation we consider tunneling as a coupling between two configurations, in the meaning that these two configurations will at some point in gate space hybridise. From the calculation of the electrostatic energy we have the eigenenergies of all the $(N+1)^D$ different charge configurations.

$$\vec{E} = \begin{pmatrix} \epsilon_{(0,0,0,0)} \\ \vdots \\ \epsilon_{(N,N,N,N)} \end{pmatrix} \tag{11}$$

The energies of all states are placed on the diagonal of a matrix, **H**. This matrix is the Hamiltonian when there is no tunnel couplings taken into consideration and only considering a double dot with a maximum of N electrons on each dot for this example.

$$\mathbf{H} = \begin{pmatrix} \epsilon_{(0,0)} & 0 & 0 & 0 \\ 0 & \epsilon_{(0,1)} & 0 & 0 \\ 0 & 0 & \ddots & 0 \\ 0 & 0 & 0 & \epsilon_{(N,N)} \end{pmatrix} \tag{12}$$

We then add a matrix with tunnel couplings placed on off-diagonal matrix elements (i,j). The coupled states follow the basic rules outlined earlier. The two different types of tunnelings will have different rates and be positioned at different off diagonal elements. This is an example of double dot with a maximum of 1 electron per dot and with coupling elements filled in.

$$\mathbf{H} = \begin{pmatrix} \epsilon_{(0,0)} & R & R & 0 \\ R & \epsilon_{(0,1)} & T & R \\ R & T & \epsilon_{(1,0)} & R \\ 0 & R & R & \epsilon_{(1,1)} \end{pmatrix} \tag{13}$$

We then calculate the eigenvalues and eigenvectors of this system. These respectively represent the energies of the hybridised states in the quantum mechanical system and what these hybridised states consist of.
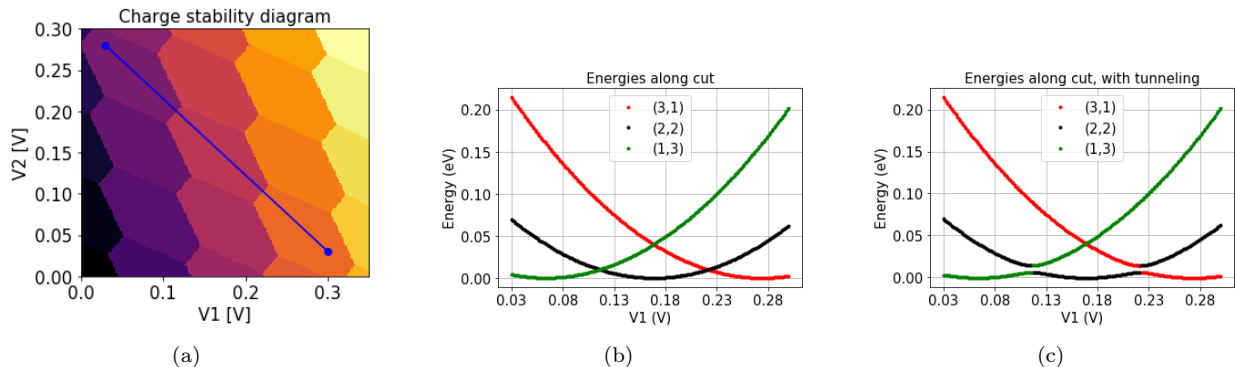


Figure 5: (a) Charge stability diagram with drawn in 1D cut (b) Energies of the three minimum energy states along cut with no tunnel coupling, and (c) Energies of hybridised state where color denote the state with the largest c-constant.

Figure 5a, show the charge stability diagram for a double dot without tunneling. The blue line on the diagional show where we take the cut that is shown in figure 5b. This plot only shows the energies of the three states (1,3),(2,2) and (3,1), and these states are also the ground states from bottom right to top left. Many other states have also been calculated for this charge stability diagram, but we are only interested in these three states to see the influence of the tunneling effect. These three states will hybridise when we introduce tunneling and the total wave function for their states is:

$$\Psi_{total} = c_{(1,3)}^2 * \Psi_{(1,3)} + c_{(2,2)}^2 * \Psi_{(2,2)} + c_{(3,1)}^2 * \Psi_{(3,1)} \tag{14}$$

When calculating the eigenvalues and eigenvectors we get the c-constants from the eigenvectors, and it is these c-constants we use to plot the charge stability diagrams with tunneling. The c-constants tell us how much of each state is present in the total wavefunction. The largest c will enable us to identify the dominating state. We use this to plot the energy of the states in figure 5c. Here we see that where the parabolas crossed in figure 5b, they now open up and join togeteher giving a smooth transition. The colors are still misleading since the green color should be very green at the first minimum and then become more and more black as it gets closer to the transition.

The same should happen with the black and the red. The red and green do not have this transition since they are not tunnel coupled in our simulation. Only (2,2) and (3,1), and (2,2) and (1,3), are tunnel coupled. In reality when the energy levels of (1,3) and (3,1) cross, there will be an anticrossing, but this is not implemented in the simulation.

There are two things we want to show with the plots of charge stability diagrams with tunneling. First we want to know what state we are in for a given set of voltages, and second we want to see a broadening at the transitions between states. We use the largest c-constant to determine the dominant state and plot this in a charge stability diagram, the concept shown in figure 5c. By doing this we can get a charge stability diagram with tunneling, that shows the specific charge states. What this does not show is the broadening. To show the broadening we plot the expected charge in one dot in a plot by it self. To calculate the expected charge in a dot we use the eigenvectors and charge states.

$$\begin{pmatrix} Q_1 \\ Q_2 \end{pmatrix} = \begin{pmatrix} 0 & 0 & ... & N_1 \\ 0 & 1 & ... & N_2 \end{pmatrix} \begin{pmatrix} c_{(0,0)}^2 \\ c_{(0,1)}^2 \\ ... \\ c_{(N_1,N_2)}^2 \end{pmatrix} \tag{15}$$

6

Using equation 15 we can determine the expected charge in dot 1 and dot 2, and the same principle applies to dot 3 and 4. The result can be seen in figure 6a and 6b.
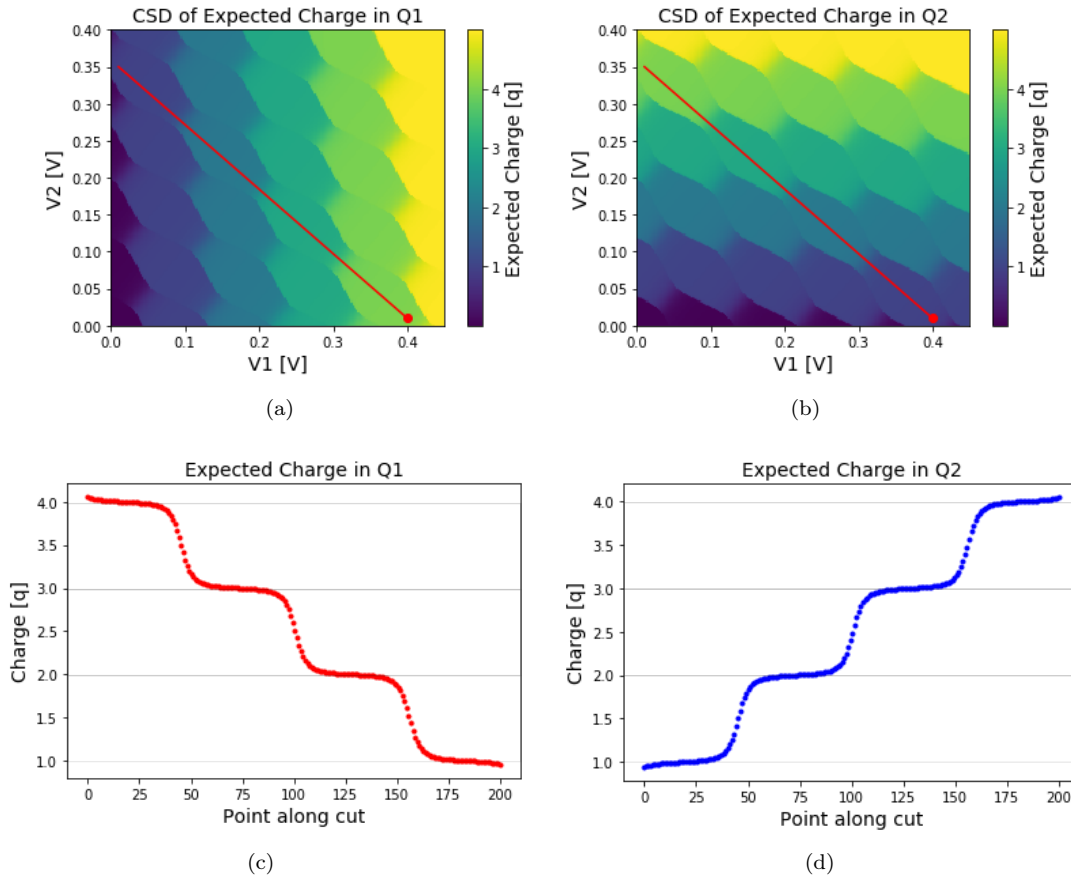


Figure 6: Expectation charge in double dot: (a) Chargestability diagram of expected charge in dot 1; (b) Chargestability diagram of expected charge in dot 2; (c) Expected charge in dot 1 along the red line; and, (d) Expected charge in dot 2 along the red line

From figure 6a and 6b, we see that the interdot charge transition is no longer discrete but has been broadened. This can also be seen in figures 6c and 6d, which show the expected charge along the red line in the charge stability diagram. Starting from the bottom right, there are four electrons in dot 1 and one electron in dot 2. As we move toward the top left of the red line, dot 1 loses an electron each time we cross an interdot transition and dot 2 gains these electrons. This results in the total charge staying the same along this diagonal band, which is five in this case. This is also true for any other parallel diagonal band, the total charge is constant when moving along a parallel diagonal.

### 2.3.1 Tunneling effects in charge stability diagrams

When tunneling is present in the simulation, it will have an effect on the shape of the diamonds in the charge stability diagram. With increasing tunnel coupling, the diamonds will become rounded edges and the interdot transition will broaden see figure 7a.

The physical interpretation of this is that with high tunnel coupling the two dots become less and less divided and finally become one dot at high tunnel coupling. So the resultant charge stability diagram is very similar to the one of a single dot see figure 7b.

The reservoir coupling also has an effect on the look of the charge stability diagram. It broadens the negatively sloped transitions, which also give a continuous transition from gaining a charge. This can be seen when plotting the expected charge in a dot.
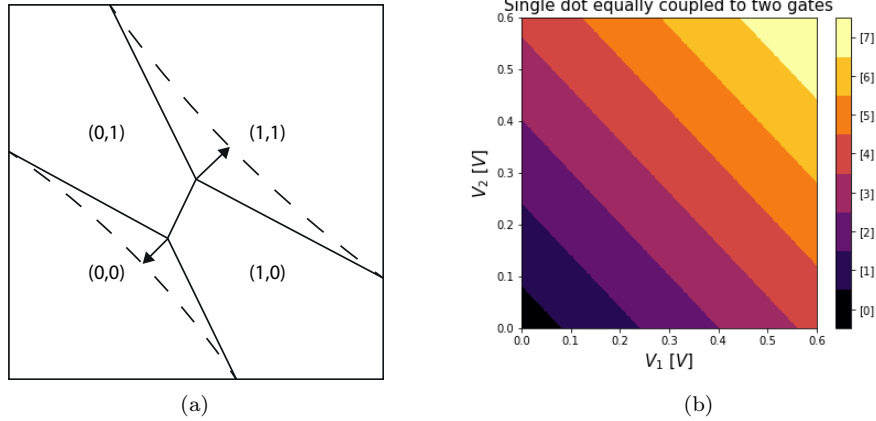
Figure 7: (a) Effect of interdot tunneling on the charge stability diagram, the interdot transitions gets wider. (b) One dot capacativily coupled to 2 gates equally.

## 2.4 Transport

Transport of electrons through the system of dots is achieved by manipulation of the chemical potential of the individual dot. The chemical potential of a dot is defined as the energy needed to add the $N_{1/2}^{th}$ electron to the dot when the system is in the $N_{1/2} - 1$ configuration.

$$\mu_1(N_1, N_2) = U(N_1, N_2) - U(N_1 - 1, N_2) \quad (16)$$

Here $\mu_1(N_1, N_2)$ is the chemical potential of dot 1 for the given $(N_1, N_2)$ configuration, likewise the chemical potential of dot 2 in the same configuration is:

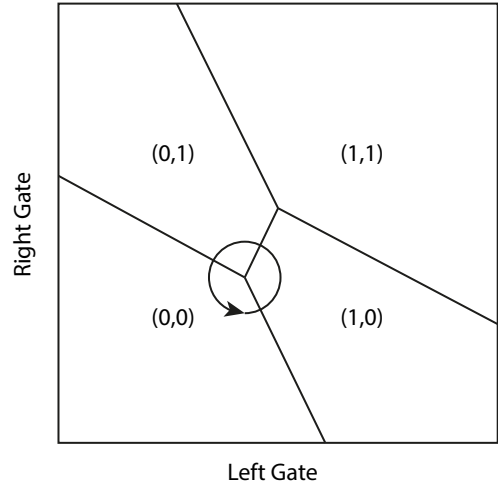$$\mu_2(N_1, N_2) = U(N_1, N_2) - U(N_1, N_2 - 1) \quad (17)$$



Figure 8: One closed loop in $(V_1, V_2)$ space (circle) pumps exactly one electron from the right to the left reservoir, when enclosing a triple point.

Our simulation does not currently calculate this chemical potential, but could be set up to do it. This is however not the only important feature of electron transport in quantum dots. The chemical potential of the leads, source and drain, are key in transportation. When the chemical potential of a dot falls below that of a nearby lead, an electron will jump from said lead onto that dot. We can use this process to transport electrons from one lead to the other, thereby driving a current across the quantum dots. One such cycle can be seen in figure 9a-9c, where moving from (a) through (b) to (c) will transport exactly one electron from the source to the drain. The manipulation of the chemical potential is realised by varying the plunger voltages, moving in gate space along the trajectory shown in figure 8. If we pulse the same trajectory around the (1,0), (1,1), (0,1) triple point, we will instead transport one electron in the opposite direction.

## 2.5 Coulomb blockade

Coulomb blockade is a classical concept based on the Coulomb repulsion between charges. This effect is present in quantum dots, as the number of electrons on a dot has an effect on nearby electrons ability to transfer on to the dot.

The coulomb barrier is the electrostatic energy barrier that electrons must overcome to enter the dot. In quantum mechanics they are also allowed to tunnel through this barrier but this effect is not considered in
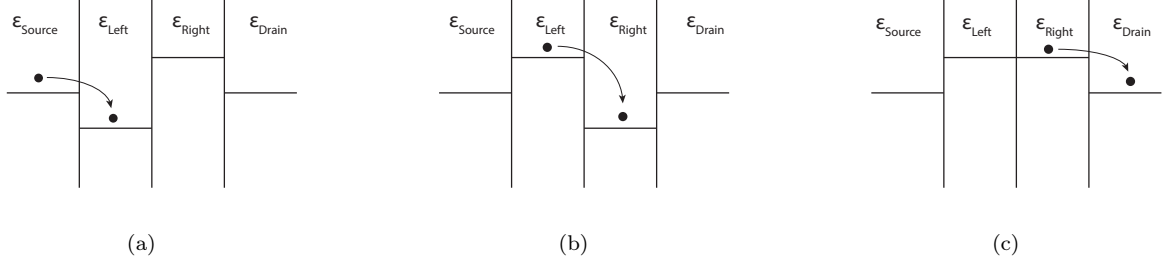
Figure 9: Electrochemical potentials of a double dot during transport cycle; (a) loading an electron on the left dot, (b) loading from left dot to right dot, (c) unloading from right dot to drain.

this section. The charging energy, the energy required to overcome the Coulomb barrier is given by:[1]

$$\Delta E_C = E_C(N+1) - E_C = \frac{e^2}{C} \tag{18}$$

Our simulation does not simulate transport, however a current measurement is the conventional way of measuring Coulomb blockade. For transport to occur we have established that the electrochemical potential must lie within the bias window, allowing electrons to overcome the Coulomb barrier. The electrochemical potential of the source, drain and dot can each be controlled with their own native gate. Our simulation does not have the bias of source and drain implemented, so we are not able to simulate this form of electron transfer, which is well established in literature. We have included a typical measurement in Appendix 8.1.

Instead we have had to resort to a different approach. We measure the charging energy as a function of gate voltage in 1 dimension. Figure 10a illustrates the minimum energy and the first excited state energy and figure 10b shows this charging energy as a function of gate voltage. Whenever the charging energy dips to zero is when there is added an extra electron. So the regions below the graph represents a constant amount of electrons on each dot.
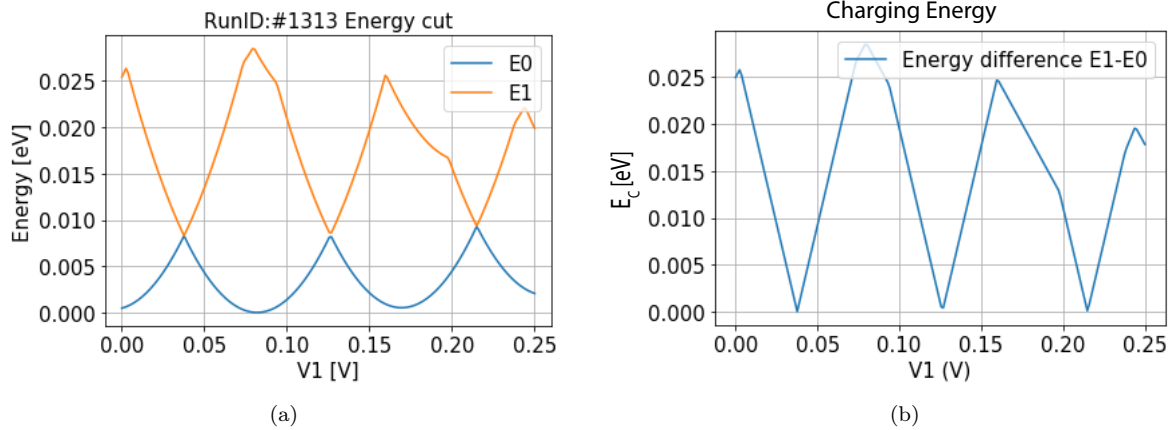


Figure 10: Coulomb Blockade (a) Minimum energy and first excited state energy of a $V_1$ cut at $V_2 = 0.075$, (b) Charging energy as a function of $V_1$, lower than our estimated $50 meV$ but this is to be expected because of other factors increasing the capacitance on the dot.

## 2.6 Reflectometry

Exploring reflectometry on a deeper level is out of the scope of this project. However since it is the primary method of measuring the quantum capacitance of a quantum dot, which most of our measurements rely on, we will briefly explain the basic principles.

Reflectometry measurements rely on measuring the reflected signal of a radio frequency wave probing a system. When an electromagnetic wave traveling through a medium experiences a change in impedance, some part of that wave will be reflected back along the opposite direction. By measuring the amplitude of this reflected wave, the impedance change of the probed system can be deduced.

In order to apply this principle to observe the behaviour of a quantum dot, we construct a tank circuit, where the capacitance of the capacitor is influenced by the quantum dot. Thereby when an electron moves onto the quantum dot, the capacitance of the capacitor changes, changing the impedance of the tank circuit which in turn influences the reflected signal.

To determine the change of impedance in the system, we use that the amplitude of the reflected signal is the amplitude of the probing signal times the gamma factor

$$A_r = A_{prob} * \Gamma \tag{19}$$

Where the gamma factor is

$$\Gamma = \frac{Z_0 - Z_{eff}}{Z_0 + Z_{eff}} \tag{20}$$
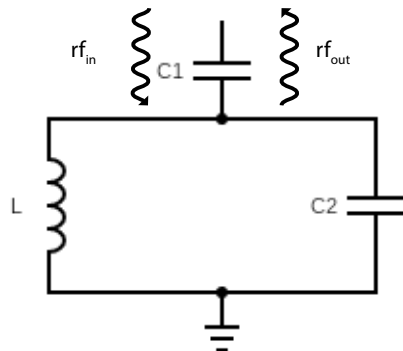


Figure 11: Tank circuit: Here C1 is the coupling to the external circuit and C2 is the capacitor that is influenced by the number of electrons on the dot[8]

Here $Z_0$ is the impedance of the source, $50\Omega$, and $Z_{eff}$ is the impedance of the tank circuit. Using these principles we can observe changes in the quantum dot by measuring the amplitude of the reflected wave.[6]

# 3 Simulation

In our bachelor project we have created a working simulation of a quadruple quantum dot, aranged in a 2-by-2 grid. We base the simulation on a capacitive model, only taking electrostatic effects into account and then add quantum mechanical effects after calculating the $0^{th}$ order energies. The simulation can be found in the references [10], and a walkthrough of the basic use of the simulation in appendix 8.2 and 8.3.

## 3.1 Topology of charge stability diagrams in 2D and 3D
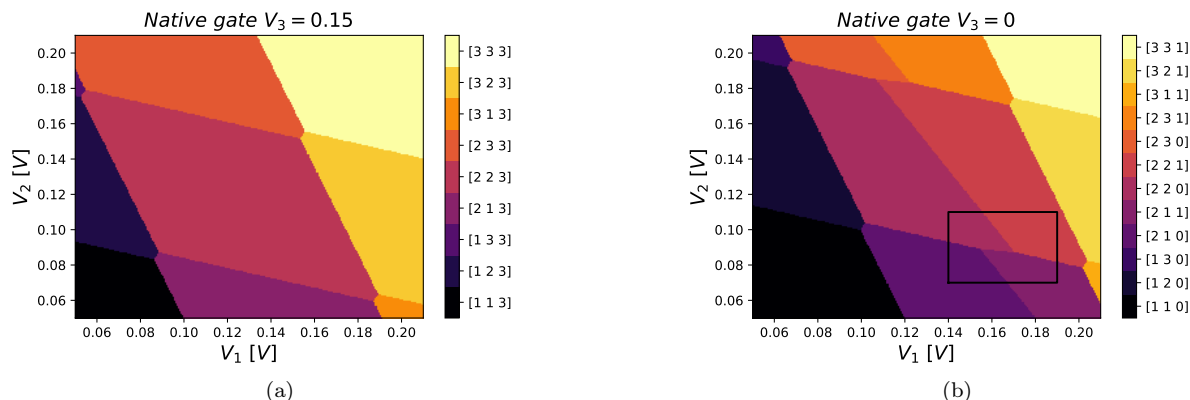


Figure 12: 2D Native gate cuts of a triple dot: (a) Charge stability diagram with $V_3 = 0.15V$, and (b) Charge stability diagram with $V_3 = 0V$, the square is enlarged in figure 13

The simulation works well for exploring the topology of charge stability diagrams. This could be done on a sample as well but would require time and stress on the sample. The exploration will hopefully uncover some interesting trajectories in gate space that can open up for exciting transport experiments.

In 2D we know that we can drive a current around a triple point, but what kind of points exists in 3 dimensions, and what physical properties are they connected to? This can be further divided into to distinct sections, one with native gate cuts, cuts along two or three physical gates, and the other with virtual gate cuts, planes in 3 dimensional gate space that can be rotated and tilted.

We start with the simplest 2 dimensional native gate cuts of 3 dots. By moving in steps along one gate while sweeping the other two, we can get a general picture of the region. Here we move in steps along gate 3 while sweeping gate 1 and 2. In figure 12 gate 3 is set to two different values, 0.15V in (a) and 0V in (b), while gate 1 and 2 are swept the range 0.05V to 0.21V. We can see an interesting effect. In 12a it shows a typical 2 dot pattern, however that is because at that combination of gate voltages the ground state will always have 3 electrons on dot 3, and we see that the shape of the (2,2,3) will have the typical hexagon shape. The hexagon is the typical state to find in a 2D native gate cut. This is because you will mainly transfer electrons in and out of 2 dots, the figure shows 6 different transitions of the (2,2,3) state which here looks similar to a two dot state.



Figure 13: Square from figure 12b showing that the (2,2,0) state is still hexagonal but with different transitions than with $V_3 = 0.15$

In figure 12b you see a clear transition through the middle of the plane, from states with 0 electrons on the 3rd dot to states with 1 electron on the third dot. This transition occurs because of the crosstalk between
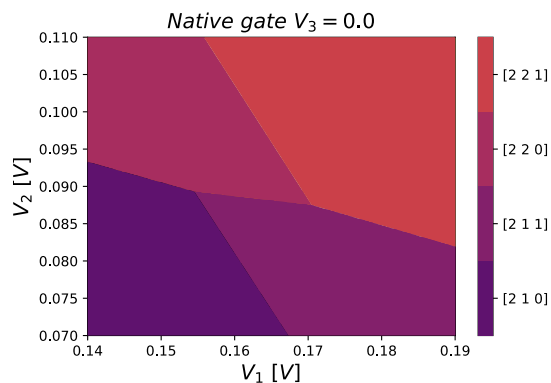
gates 1/2 and dot 3. It is not present in the case where $V_3 = 0.15V$, because we here moved gate 3 to 0.15V and the crosstalk is not strong enough in this region of gate space to get the 4th electron to transfer on. The square in figure 12b is enhanced in figure 13 to show that the (2,2,3) state still has a hexagonal shape, the zoomed in version shows that it is not a straight line and therefore a hexagon. Here a reservoir transition and an interdot tunneling transition are connected to dot 3 instead of dot 2.

These figures show the dependence of transitions on all three gates simultaneously, showing that our simulation is working as intended with respect to cross talk between dots and plunger gates. As you move around the 3 dimensional gate space some cuts will be more interesting than others. A general point of interest will be the aforementioned triple points. But "moving" these transitions around can open up for a lot of discussion and questions.

Another way of exploring the 3 dimensional gate space is by plotting in 3 dimensions. This way one can obtain a more intuitive view of the states. The charge stability diagram for three quantum dots can be interpreted similarly to the charge stability diagram of a double dot. The only difference being that there is an extra dimension. This third dimension also gives the diamond islands from the two dimensional charge stability diagram an extra dimension, which makes them quite a bit harder to visualise. If we use the same approach as we used in the two dimensional charge stability diagram, we can visualise the shape, by considering the neighbouring states. The number of neighbouring states was the number of ways we can change a state configuration by moving one electron. Each of the dots can either gain or lose an electron to the reservoir. There are three dots, this gives us six neighbours. The electrons can also move between
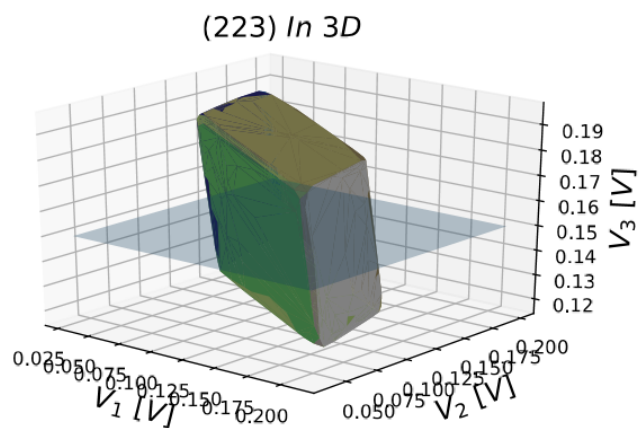


Figure 14: A 3 dimensional plot of the (2,2,3) state where the cubelike figure clearly shows, there is also added a plane to show where the cut from figure 12a is taken

dots. Back and forth between dot 1 and 2, 2 and 3, and 1 and 3. This gives us another six neighbouring states to a total of 12 neighbouring states. From this we can assume that the three dimensional potato will have 12 facets. This is however only for the symmetrical configuration of the array, in a linear triple dot we have found there to be a total of 14 facets. The two new facets being added are double transitions, where a reservoir transition and an interdot transition occurs. To accomplish this we have used an algorithm that sweeps outward from a point and move the direction along the surface of a sphere. When choosing a starting point in the central part of a given state, one can get a clear form of that state, which then can be plotted using a convex hull algorithm. The radial search algorithm works by moving in some direction and measuring at set intervals, when it encounters a different state than the one it started in, it will send back that point and return to starting point for moving in a different direction. The result can be seen in figure 14 where the (2,2,3) state is plotted using this method. Here you can also see why a cut in $V_1, V_2$ gate space will have many states looking like hexagons. The added plane is the cut taken in figure 13.

In figure 15 we show a collection of cuts through the region in native gate space that contains the (111) charge state. We here see the various shapes it appears as, ranging from a triangle in figure 15h to an octagon in 15b. This was done by performing 8 two dimensional sweeps of gate 1 and 2 while changing gate 3 between each sweep. We also show the same measurement in appendix 9.4 but with the complete charge stability diagram.
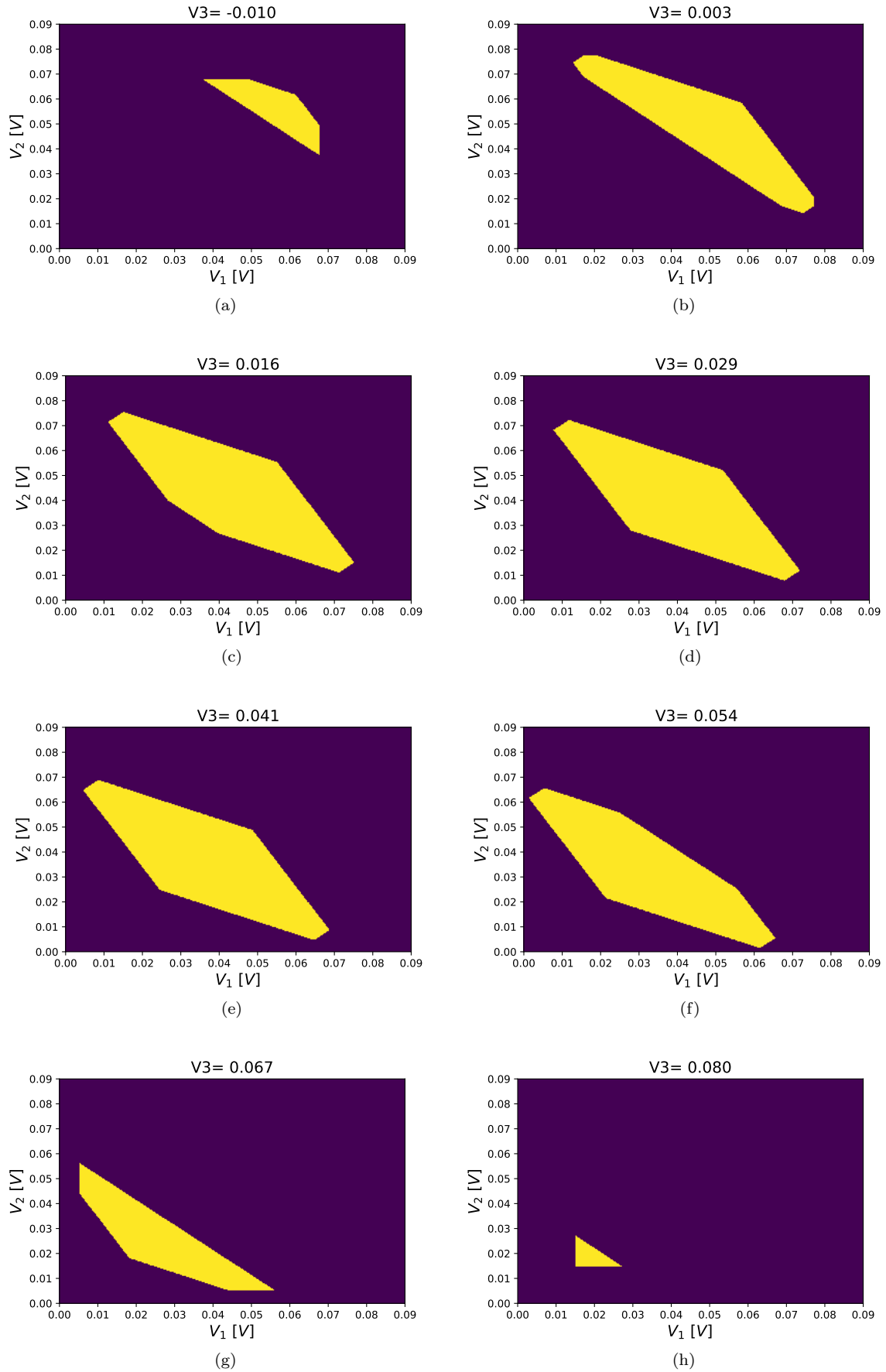
Figure 15: Multiple cuts of the (111) region in native gate space, with cuts taken at different values of the native gate 3, while sweeping gate 1 and gate 2

The last method of exploring the 3D gate space is through virtual gates Here we can define a different coordinate system to sweep in. For most purposes a rotated cartesian coordinate system will be sufficient. This can be obtained by this relation,

$$\vec{V}_v = \mathbf{\Theta}\vec{V} = \begin{pmatrix} \theta_{11} & \theta_{12} & \theta_{13} \\ \theta_{21} & \theta_{22} & \theta_{23} \\ \theta_{31} & \theta_{32} & \theta_{33} \end{pmatrix} \vec{V} \qquad (21)$$

$\vec{V}_v$ is the virtual gate and $\vec{V}$ is the native gate voltages, and $\theta_{ij}$ is the $i^{th}$ basis vectors $j^{th}$ coordinate in real gates. We have taken multiple measurements along the common mode, $\begin{pmatrix} 1 \\ 1 \\ 1 \end{pmatrix}$, because the endpoints of the (1,1,1),(2,2,2)... states are roughly following this common mode. The normalized common mode matrix looks like:



Figure 16: Virtual sweep of gate space, the plane of the sweep is perpendicular to the common mode, this is a good angle for sweeps of any of the (n,n,n) regions since they are all fairly close to the common mode.

$$\Theta_{Common} = \begin{pmatrix} \dfrac{1}{\sqrt{3}} & \dfrac{1}{\sqrt{3}} & \dfrac{1}{\sqrt{3}} \\ \dfrac{-1}{\sqrt{2}} & \dfrac{1}{\sqrt{2}} & 0 \\ \dfrac{1}{\sqrt{6}} & \dfrac{1}{\sqrt{6}} & \dfrac{-2}{\sqrt{6}} \end{pmatrix} \qquad (22)$$

By inverting the matrix we can move in this virtual space and send real values to the actual gates $\vec{V} = \Theta_{Common}^{-1}\vec{V}_v$. This allows us to move along the common mode and take sweeps of the 2 virtual gates. This opens up a possibility of finding interesting shapes of states. In figure 16 the (111) state appears with 12 different bordering states, where 1 is so small it is difficult to see in the bottom right corner of the (111) state. When moving along the common mode this state will appear smaller and smaller until we move into the (222) state, but when the state is a small triangle it serves as a good working point for moving holes around, which will be expanded upon in the section on simulating electron exchange in a triple dot below.

Figure 32 shows the same type of measurement as figure 16, multiple sweeps of the perpendicular axis to the common mode. Again we can see the many different shapes that a charge state can appear as in two dimensional sweeps, the triangle often appears and is quite useful but this will be expanded upon in sec. 3.4. With a large amount of sweeps we can make a video showing the expansion of the charge state that occurs when moving along this direction. We also have the full charge stability diagram of this measurement in appendix 9.4.
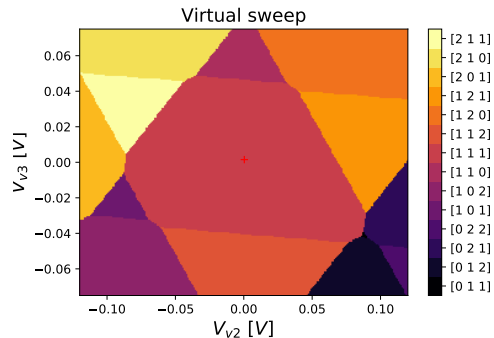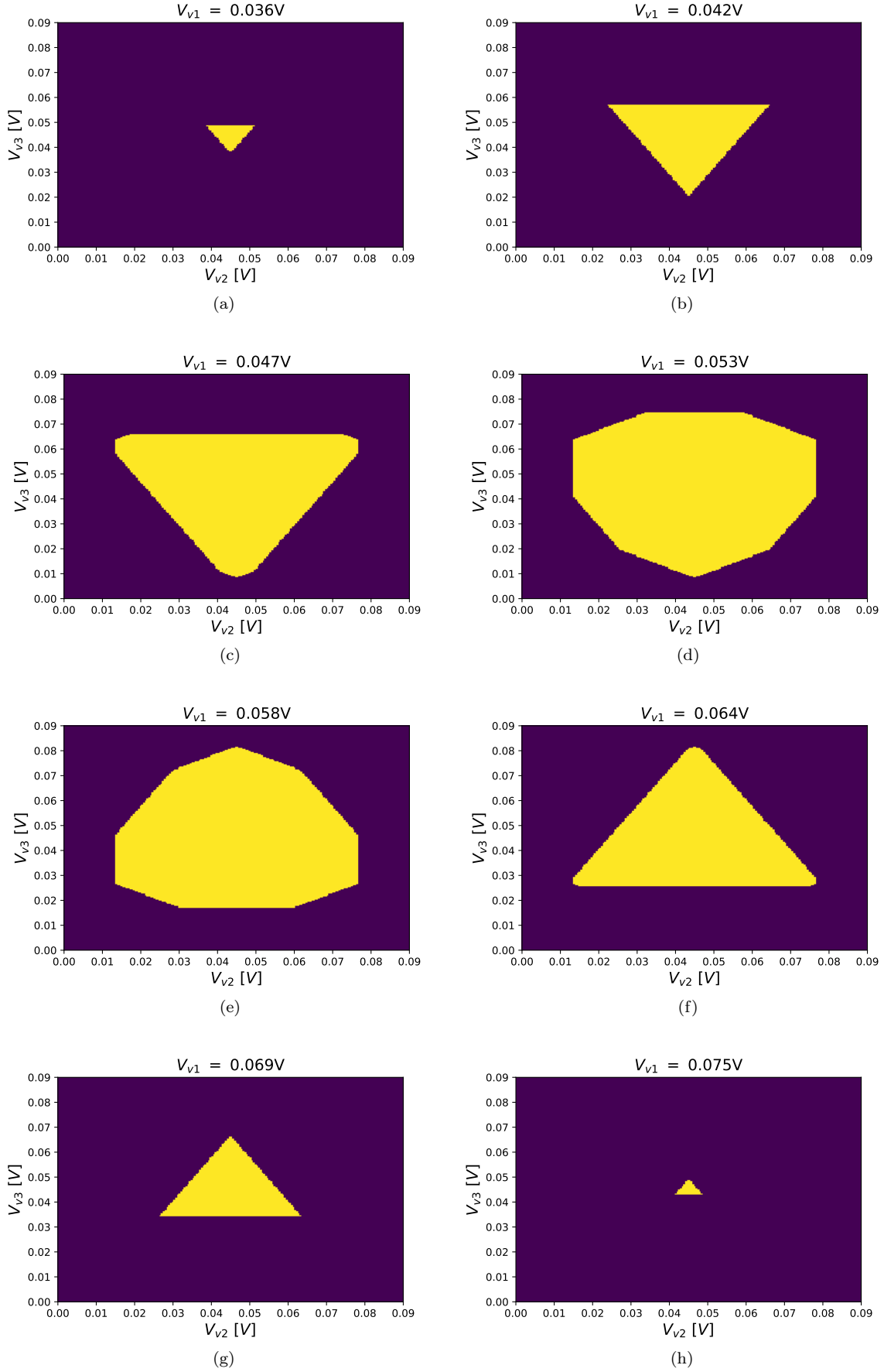
Figure 17: Various cuts of the (111) region taking at different values of the common mode and sweeping virtuel gates that are perpendicular to the common mode.
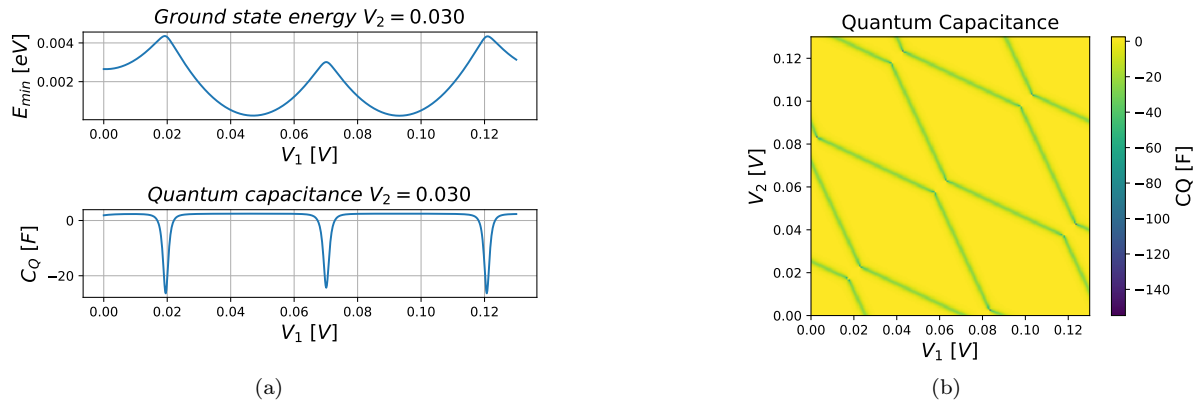
## 3.2 Quantum Capacitance



(a)



(b)

Figure 18: Quantum capacitance: (a) the ground state energy and the calculated quantum capacitance, with dips where transitions between charge configurations occur, (b) A 2D map of quantum capacitance, derived with respect to gate 4 (kept at 0.1V) while sweeping gate 1 and 2

The quantum capacitance is an intrinsic property of all conducting materials. Reflectometry measures the quantum capacitance, so we wanted the simulation to be able to reproduce measurements that look like actual reflectometry data. The quantum capacitance, $C_Q$, can be found from the second derivative of the energy [9]:

$$C_Q = \frac{\delta^2 E}{\delta V^2} \tag{23}$$

This is achieved by numerical derivation with respect to a specific plunger gate, in application it will usually be with respect to gate 4. Dot 4 is often being used as a sensor dot for taking measurements on a 3 dot system. In figure 18a you can see a measurement of ground state energy and quantum capacitance. Here the quantum capacitance is taken with respect to gate 1, which is also the gate being swept. You will also see the slow increase in ground state energy as $V_1$ increases. This is due to the effect of $V_2$ skewing the honey comb. The cross talk interferes and as gate 1 increases it comes closer to a transition in dot 2. If there existed no cross talk, the honeycombs would be squares and the minimum energy would be perfect parabolas with the same local minimum.

When looking at 2 dimensional maps it is however more suitable to find the quantum capacitance with respect to a gate not being swept. In figure 18b the quantum capacitance is taken with respect to gate 4, this is done to make it resemble an experimental setup where the reflectrometry measurements requires a nearby quantum point contact.

Another option shown in figure 19 is calculating the derivative with respect to gate 1. Here we see a clear distinction between the transition in the dot closest to the swept gate, and in the transition in the dot furthest away from the swept gate.
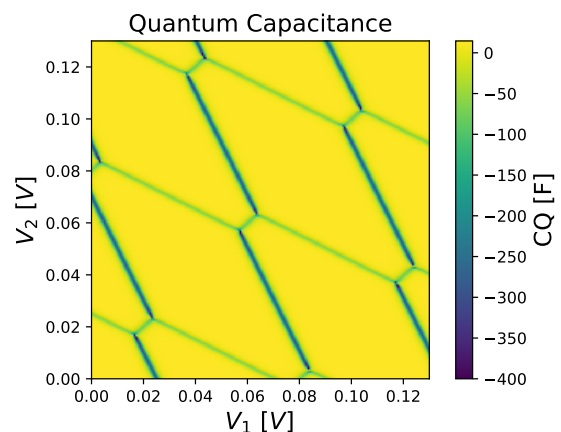


Figure 19: Quantum capacitance calculated with respect to gate 1, here with a cutoff of -400 implemented for better visibility in total there is 73 points $<=$ -400 in this 400x400 map.
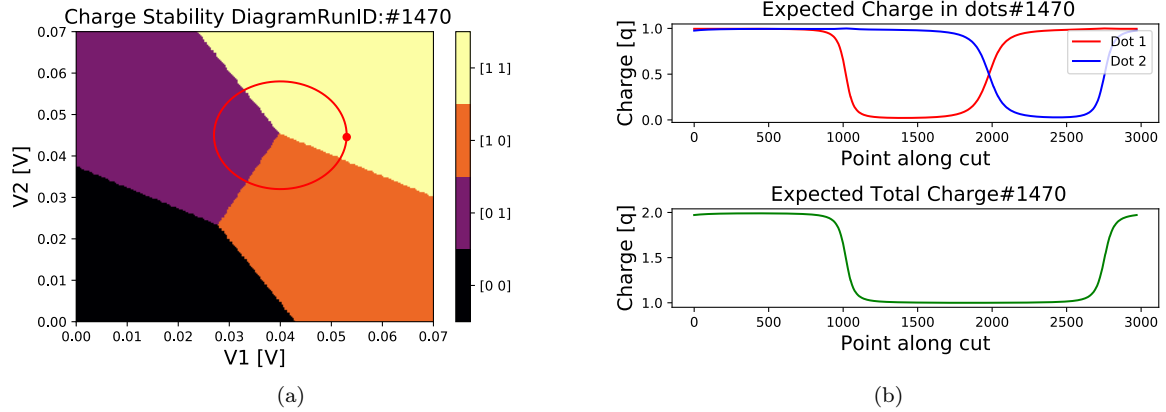
## 3.3   Simulating double dot transport



Figure 20: Transport simulation (a) shows the charge stability diagram with a circular trajectory around one of the triple points. (b) shows the expected charge in each dot and the total charge in the system

The simulation is not set up to actually measure transport. Instead our solution is to plot the expected charge in dot 1 or 2 when pulsing along a trajectory. In figure 20a we show the trajectory with the working point marked by a dot and direction going counterclockwise. In this measurement we expect a single electron to be transported per cycle. This can be seen from figure 20b where we show 1 cycle of gate voltages. Here we clearly see that there is only one transition per cycle during which the two dots exchange an electron.
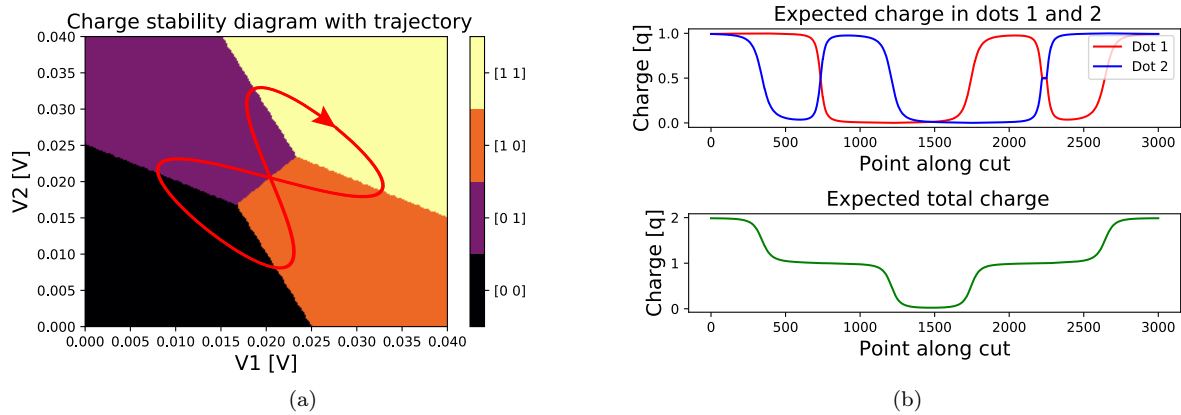


Figure 21: Transport simulation of Lissajous (a) charge stability map with Lissajous trajectory starting point of the trajectory is indicated by the arrow (b) the expected charge in individual dots and combined, the total transfer of electrons is 2.

In figure 21a we show the tilted Lissajous we also use in the section on Lissajous driving of single electrons and we measure the expected charge at each point along this trajectory going clockwise around the bottom loop and counter clockwise around the top. In figure 21b we see that there are 2 transitions where the dots exchange an electron, the second transition happens at the beginning/end of each cycle which is not shown that well in the graph. So at this working point we would expect to see double the current if driven with the same period as the circle in figure 20a.

## 3.4   Simulating electron exchange in a triple dot

When doing a tilted two dimensional cut through the three dimensional gate space, we see shapes that we have not seen when doing native gate sweeps in the two dimensional gate space. One of these shapes is a

triangle, which appears when we do a cut through one of the corners of the three dimensional diamonds.

Depending on which corner the tilted cut goes through, the bordering states will either have one less electron on one of its dots or one more electron on one of its dot. If the cut is taken through the corner closest to the origin, and the (0,0,0)-state, the three bordering states will have one less electron than the triangle state. If the cut is taken through the corner far from the origin and the (0,0,0)-state, the three bordering states will have one more electron than the triangle state.

In figure22a the (1,1,1) - state can be seen as a triangle in the middle. Starting from the state with the red dot and going counter clockwise the three bordering states are, (1,1,0), (0,1,1) and (1,0,1). Figure 22a is the charge stability diagram that shows the most dominant state, in the total hybridised state. The three charge stability diagrams below, figure 22b, 22d and 22f, show the expected charge in respectively dot 1, 2 and 3. In these figures it is not obvious that the (1,1,1)-state is in the middle, but what they do show is the broadened transition between states. The empty space that is being moved around during the exchange, can also be seen here as the dark blue areas. In the charge stability diagram for quantum dot 1 the charge goes from zero charge in the top area to almost two charges in the bottom yellow area.

It is along the red circle that we measure the expected charge in the three quantum dots. The measurement does two periods of the circle, and the expected charge along the circle is shown in the three figures to the right of the expected charge maps, figure 22c,22e and 22g. From the three figures we see that we start with one electron in dot 1 and 2, and zero electrons in dot 3, the (1,1,0)-state. The electron in dot 1 then moves to dot 3, and the system is in the (0,1,1)-state. The electron in dot 2 then moves to dot 1 and then the electron in dot 3 moves to dot 2. The two electrons that started in dot 1 and 2 have exchanged places. This process is a big part of quantum computing since it allows for the exchange of 2 spins, if the 2 electrons start in a entangled state they will remain entangled throughout the exchange and therefore will keep their spin orientation. This phenomenon can then be investigated by applying a magnetic field to probe the spins.

(a)



(b)



(c)



(d)



(e)



(f)



(g)

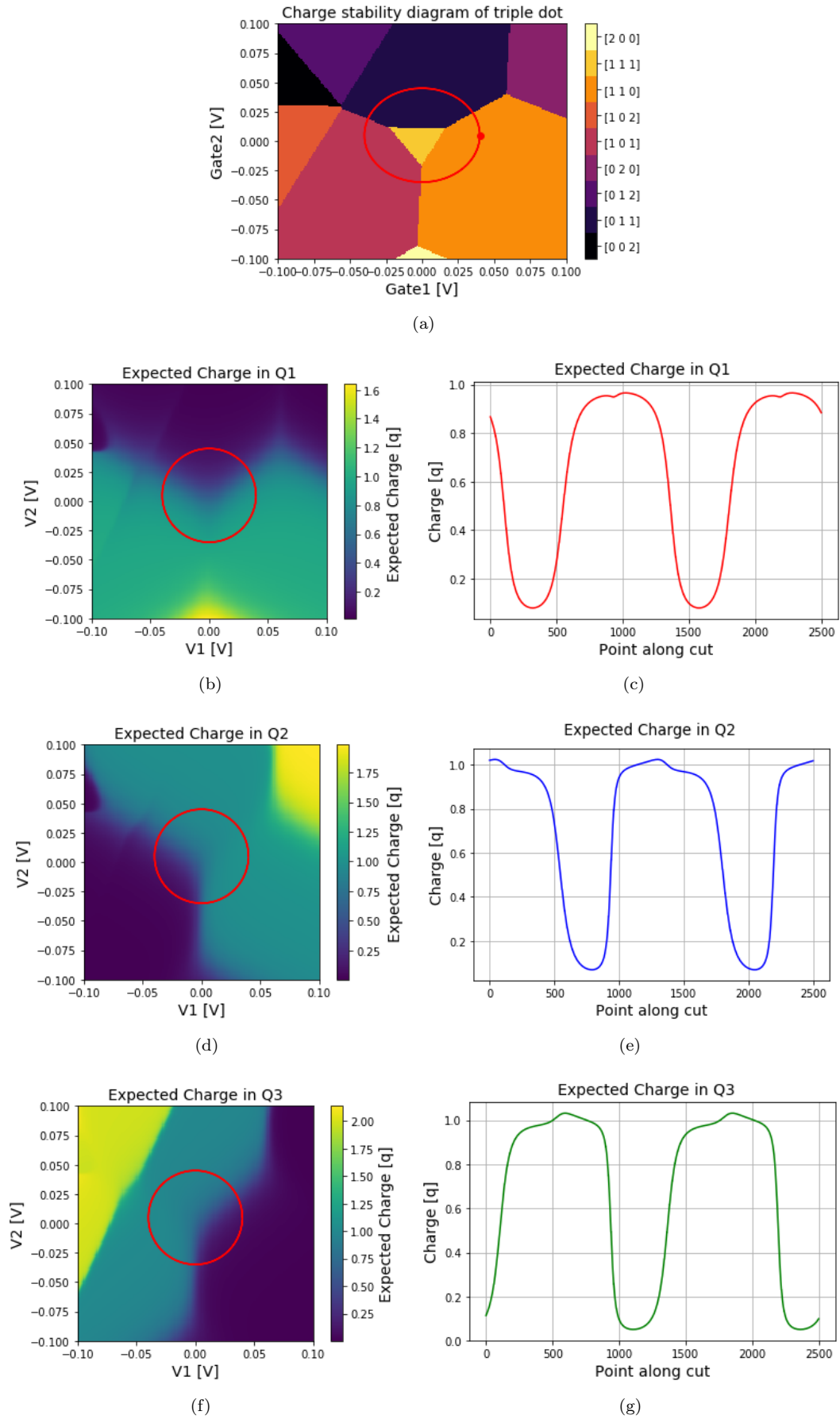Figure 22: Exchange of two electrons in real space: (a) Charge stability diagram with trajectory; (b) Charge stability diagram of expected charge in dot 1; (c) Expected charge in dot 1 along the red circle; (d) Charge stability diagram of expected charge in dot 2; (e) Expected charge in dot 2 along the red circle; (f) Charge stability diagram of expected charge in dot 3; and, (g) Expected charge in dot 3 along the red circle.

19

# 4 Device

In this project we worked with two devices, a gallium arsenide based device and a silicon based device. The gallium arsenide devices was used to do the transport experiments in section 5 and it was measurements from the silicon device we used in section 2.2.1 to extract capacitances.



<div align="center">(a)</div>
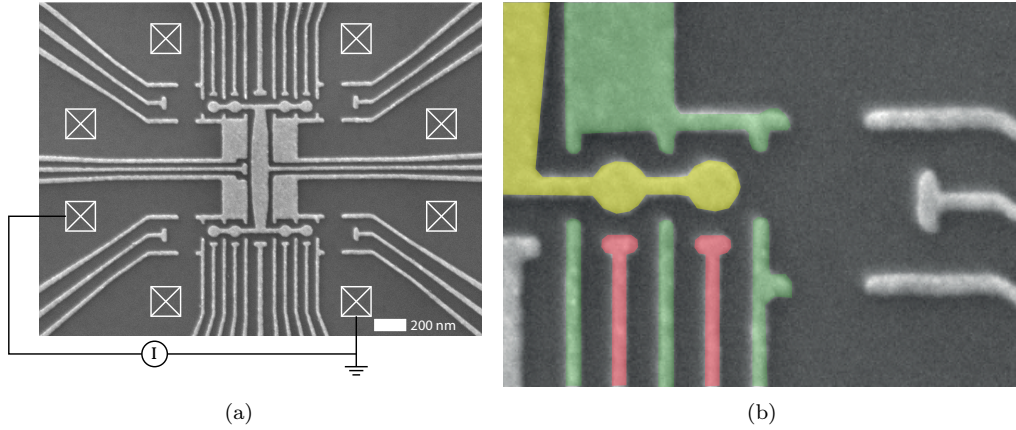
<div align="center">(b)</div>

Figure 23: FF1B: (a) The entire FF1B device with all gates visible and, (b) a zoomed in picture of one of the double dot regions with plunger gates in red, barrier gates in green and the dots/jellybean in yellow.

The gallium arsenide device consists of four double dots, which are formed in the material beneath the circular areas, which are highlighted in figure 23b as yellow. The four double dots are connected by a jellybean (named after its shape), which is used as a reservoir and an area for electrons to move freely between the four double dots.

By applying a positive voltage over the yellow gate we can attract electrons to the area beneath it, and using the green and red gates we can further manipulate each of the dots. The green gates are called barrier gates. They are used to better define the shape of the dots and in turn the tunnel coupling between dots. This can be done by applying a negative voltage to the barrier gates which repels electrons from the area around it. The red gates are called plunger gates. These gates are used to manipulate the number of electrons on the dot, by either applying a more positive voltage to attract electrons or a more negative voltage to repel electrons. In figure 23b there are also eight white squares with a cross. These indicate the ohmic conducts, which can be used to apply a bias in order to direct a current through the device.

The other device we worked with was the silicon device. The silicon device has four gates, shown in white, each of which control and form a quantum dot in a nanowire beneath them. The nanowire is made of very pure silicon and at each of its ends it widens out to the two large dark rectangular areas. These two dark rectangles stem from the same layer of silicon as the nanowire, but have been doped with phosphorous to free electrons, making them semiconductors, so they can be used as source and drain.
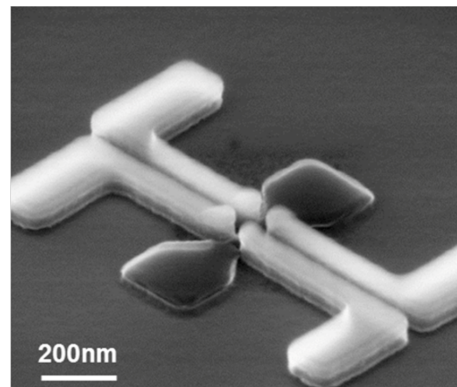


Figure 24: SEM of a silicon device identical to the one we worked with.

# 5 Lissajous driving of single electrons

On the 20th of May 2019 the SI-units were redefined, one of which is the ampere, the unit for current. It was previously defined by a constant current flowing through 2 infinite conductors, that induces a force between the two conductors of a specific magnitude. It has been redefined by fixing the numerical value of the elementary charge to be $1.602176634 \cdot 10^{-19}C$ and defining the second to be $\Delta v_{C_s} = 9192631770s^{-1}$, the hyperfine structure transition frequency of caesium-133. Using the relation between ampere, coulomb and seconds $A = \dfrac{C}{s}$, the ampere is now expressed as:

$$1A = \frac{e \cdot \Delta v_{C_s}}{1.602176634 \cdot 10^{-19} \cdot 9192631770} \tag{24}$$

this can be thought of as a measure of how many electrons are being transported in one second.

In this section we will investigate quantized currents and show that by moving along certain trajectories in gate space, we can move 1 electron at a time, and by changing the period of the trajectory we can change the measured current. Some of the trajectories used will be lissajous curves, introducing exciting properties of the various trajectories.

## 5.1 Method



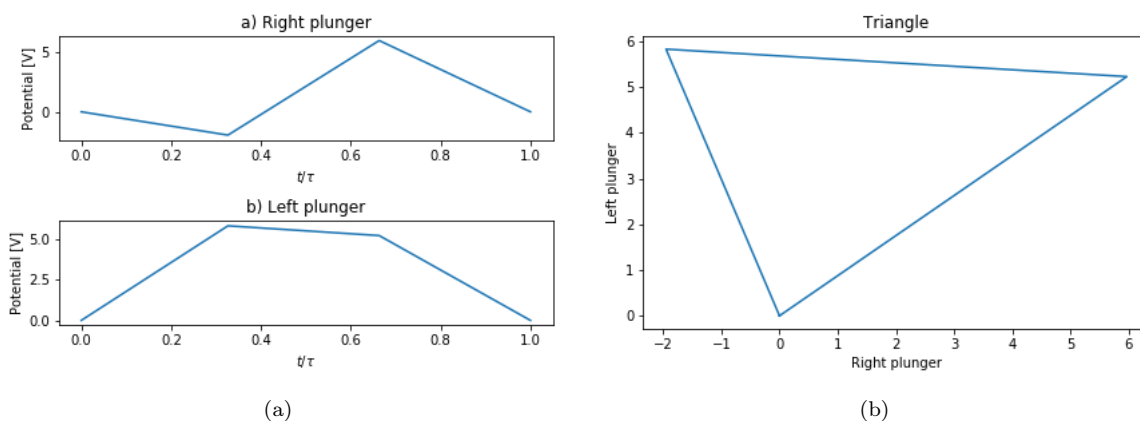(a)                                        (b)

Figure 25: Building a trajectory: (a) The cycle for individual plungers, and (b) The trajectory in gate space.

We apply an alternating voltage to the two sweeping gates on top of the already applied constant voltage, such that each gate will be $DC + AC$. The DC plunger gates act as a working point from where the trajectory starts. By analysing the path we can predict what working points will induce source-drain current and which will not. Further it can be predicted which direction the current will be running. We measure electrons being transported from source to drain as a positive current. Where source and drain is two of the ohmic conducts shown in figure 23a.

This allows you to chose a trajectory in gate space and explore the transport of that trajectory. This is particularly interesting when the trajectory encloses a triple point. When you move around a triple point you will drive a current from the source to the drain or in reverse depending on your direction around the triple point. Figure 20a above shows a transport simulation with a circular trajectory around a triple point. When going counter clockwise around
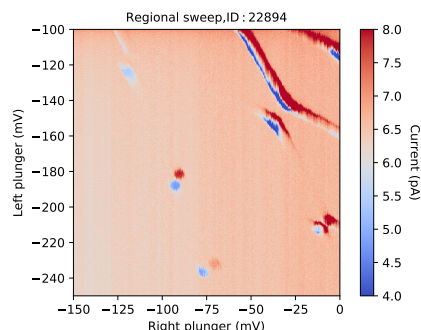


Figure 26: Big charge stability diagram of the device in the working configuration for the transport experiment, no trajectory is driven here this is only DC being swept.

point B you will drive a positive current by going through the three states as: $(1,0) \rightarrow (1,1) \rightarrow (0,1) \rightarrow (1,0)$. Thereby moving 1 electron from the source to drain. When we perform this trajectory many times it will constitute a quantised current. For our measurements the alternating voltage typically has a frequency of $10MHz$, which will drive a current of $10MHz \cdot (1.602 \cdot 10^{-19}C) = 1.602 \cdot 10^{-12}A$. We also measure what happens when the trajectory becomes big enough to enclose both triple points when measuring at specific working points (between the triple points). Here we move through 4 states as: $(1,0) \rightarrow (1,1) \rightarrow (0,1) \rightarrow (0,0) \rightarrow (1,0)$. This however does not drive a current. Instead of 1 electron tunneling through both dots from source to drain or opposite, there will instead be one electron exchange between the source/drain and its nearest quantum dot. So at the first arrow there will tunnel 1 electron from source/drain onto the left dot. At the second the 1 electron already on the right dot tunnels out to the source/drain, third arrow, the left dots electron tunnels out and fourth arrow the right dot gets 1 electron from source/drain, which completes the cycle.

We can also choose a more complicated trajectory that will have some interesting features. For example what will happen when we enclose both triple points in the cycle but move in opposite direction around them? As you can see from figure 21a we will actually transport 2 electrons instead of just 1 through a cycle.

This is also where the Lissajous figures comes into play. They are handy to work with since it is very easy to produce sine wave modulated pulses. Figure 27 shows how a lissajous figure can be prepared for a measurement, a) and b) shows the pulses on the right and left plunger to produce the desired $\infty$ trajectory. These are $Rp = sin(x)$ and $Lp = sin(2x)$. Then by applying the rotation matrix.

$$R(\theta) = \begin{pmatrix} cos(\theta) & -sin(\theta) \\ sin(\theta) & cos(\theta) \end{pmatrix} \quad (25)$$



Figure 27: Building the lissajous figure trajectory, (a) and (b) shows the voltage on individual plungers, (c) the complete lissajous and (d) a figure rotated by 240°

on the plunger gates, $\begin{pmatrix} Rp \\ Lp \end{pmatrix} = \begin{pmatrix} sin(x) \\ sin(2x) \end{pmatrix}$ , we rotate in the coordinate system to get a trajectory capable of enclosing both triple points at the same time.

## 5.2 Results



(a)
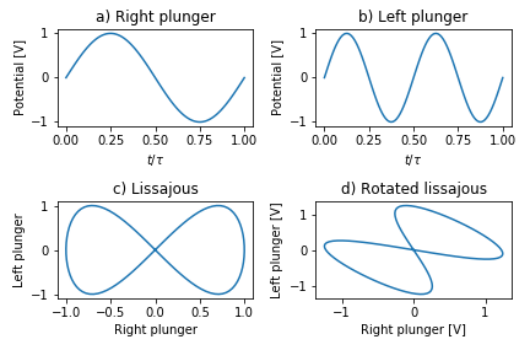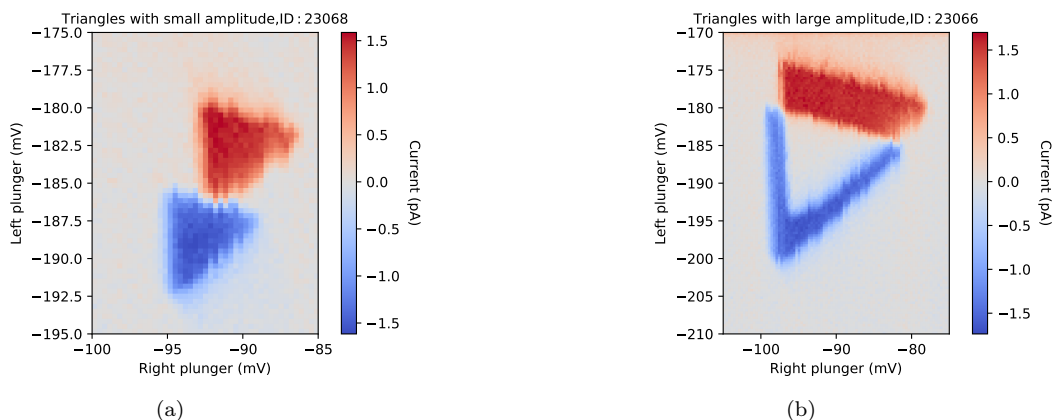


(b)

Figure 28: Single electron current driving; (a) triangles in gate space, with length=6mV showing current driven around triple points, and (b) triangles with length 18mV showing no current when both triple points are enclosed in trajectory

Figure 25a show the individual gate pulses of a triangle in gate space with an amplitude of about 6mV. Figure 25b show for the resulting triangle in gate space. This triangle was driven in the region around the triple points located at $(-90, -180)$ in fig. 26.

In figure 28a we show the result of this trajectory taken at working points within the $(-100, -195)$ to $(-85, -175)$ region. This pulse is driven at 10Mhz, so each pulse cycle is $100ns$ and with a ramp on every section. The ramp ensures a smooth trajectory even if the 2 plunger gates are slightly out of phase. We predicted a driving current of $1.6pA$ and the data supports it very well. We also see that it drives negative current around 1 triple point and positive current around the other, this is expected because the trajectory around one triple point transports an electron from source to drain and the same trajectory around the other triple point will transport from drain to source, see sec. 2.4.

Now we increase the amplitude of the triangle 3 times. This means that when your working point is between the two triple points, both of them will be enclosed in the trajectory. Figure 28b clearly shows that there is no transport of electrons when both triple points are enclosed in the loop. There is no current measured because the trajectory is not crossing the interdot transition, meaning that the only exchange of electrons is between dot and reservoir.

In figure 29 you can see a tilted Lissajous corresponding to the Lissajous in figure 27, with a rotational angle of $\theta = 240°$. This also has the property of enclosing both triple points, however here the direction around each triple point is opposite each other. This results in double the amount electrons being transported in the same direction, measuring twice the current. Which is clear from the colorbar, the biggest negative current is still at -1.5pA while the biggest positive current has increased to close to 3pA. We however still see some regions of positive current consistent with the transport of 1 electron.
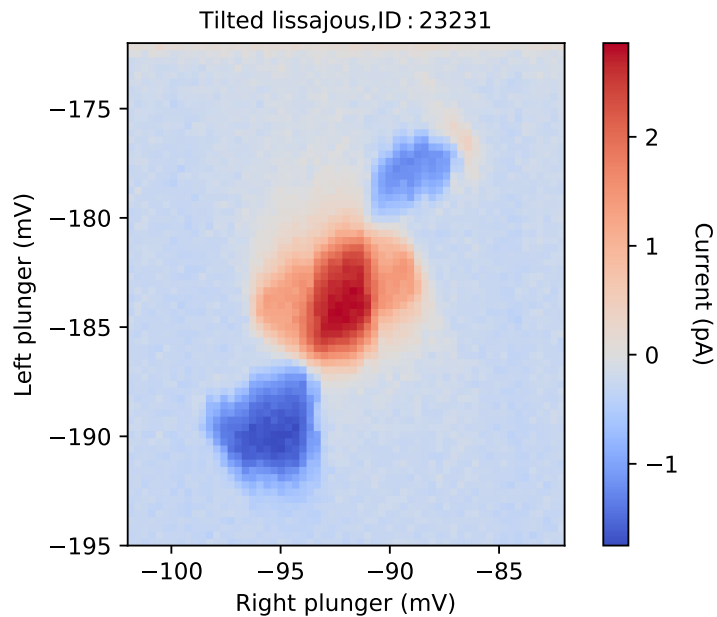


Figure 29: Lissajous figure rotated by $\theta = 240$ and with an amplitude of 6mV

# 6  Discussion

We have developed software that can simulate various types of measurements applicable to quantum dots in arrays. We would like to review them in this section. The charge configuration measurement and specifically the charge stability diagram, is useful because it gives a very intuitive feel for working with quantum dots. Also it is great at characterizing devices if you know their capacitive couplings. However it should ultimately not be considered the most important result of the simulation. There are some problems with the charge stability diagrams as they give a false sense of certainty. When working from a point close to a transition, our charge stability diagrams leads you to believe that you still are in that specific state, when actually the system will be in a superposition of multiple different configurations. Here the expected charge measurement accounts much better for quantum mechanical effects, while still keeping an intact intuitive understanding. The charge stability measurement is however useful in other types of measurements, the radial search type of measurement, or more general when you want to explore just 1 configuration.

The problem for radial search is that you have to find the midpoint quite precisely for the best measurements. And even then the method is bad at displaying corners. The corners are typically the farthest away points from the centre and there will be a smaller amount of points per surface area on the corners. The corners are the most physically interesting points to explore. Making an adaptive method for changing the directional step would go a long way in solving this, it however requires a means of figuring out when you are at a corner or more generally an area with high curvature. Another good inclusion in this code would be to merge the first plots colorbar with the 3 dimensional plots so it would be easier to recognize which states are bordering up to each other there. Unfortunately there are also some unintentional transparency effects when plotting using this method, it seems however to be a problem with how matplotlib is built. We could investigate other packages to find a better solution.

Making a calculation for the transport of electrons through the system seems like a feature we with sufficient time could implement. We could use the calculated electrostatic energies to calculate the chemical potentials on the individual dots. Further we could define some Fermi level and base transport on whether the chemical potential of a dot lies within the bias window or outside. Another way could be to base the simulation on something other than electrostatics entirely.

We also implemented a form of quantum capacitance, which is useful for comparing the simulated data with data from real instruments. We would have liked to explore this measurement further to also try and use a compensated reflectometry gate for getting specific states to appear lit up. This could be the most important measurement going forward, since it is the one most resembling real data.

The method we used for extraction of capacitances is perharps a bit too simple for the complicated devices used. In the devices the quantum dots are electrostatically defined by gates that are not accounted for in our model, so this method will give results that might get the right ratio between gate capacitances, but might be either too small or too big. There is also an issue regarding the data for some of the capacitances. Some of the data sets used did not have clean native gate cuts, but rather compensated sweeps of composite gates.

## 6.1  Outlook

The simulation is a basis to work further off, there are many possibilities for how to proceed and what to use it for. Some applications lie within machine learning. It could be used to produce training sets for artificial intelligence. Today the training sets used by artificial intelligence is already a mix of real data and simulated data. [7] This simulation could be a tool in the process of simulating more data, further development would though be required. The artificial intelligence is trained to recognize configurations, and to adjust gate voltages, to get into a desired configuration. By getting better AI we would be able to advance faster in quantum technology by eliminating a lot of required set-up time when conducting experiments on quantum dots. It could potentially also work as a device investigator, in the sense that it could be trained to reproduce real data sets based on the supplied voltages. Instead of figuring out the locations in gate space we could calculate the actual capacitive couplings within a device.

# 7    References

# References

[1] Thomas Ihn. *Semiconductor Nanostructures.* Oxford University Press, 2010.

[2] Yuli V. Nazarov, Yaroslaw M. Blanter. *Quantum Transport* Cambridge University Press, 2009.

[3] Tero T. Heikkilä. *The Physics of Nanoelectronics.* Oxford University Press, 2013.

[4] W. G. van der Wiel. *Electron transport through double quantum dots.* Reviews of Mordern Physics, Volume 75, p. 1-22, 2003.

[5] Neil P. Oxtoby *Model for monitoring of a charge qubit using a radio-frequency quantum point contact including experimental imperfections* Phys. Rev. B 77, 125304 (2008) https://arxiv.org/abs/0706.3527

[6] Bruno Küng *RF Reflectometry Measurements of Quantum Dots.* Zurich Instruments, 20th February, 2017. https://www.zhinst.com/blogs/brunok/rf-reflectometry-quantum-dots/

[7] D. T. Lennon, H. Moon, L. C. Camenzind, L. Yu, D. M. Zumb¨uhl, G. A. D. Briggs, M. A. Osborne, E. A. Laird, and N. Ares. Efficiently measuring a quantum device using machine learning. arXiv preprint http://arxiv.org/abs/1810.10042 , 2018.

[8] Imtiaz Ahmed *Radio-Frequency Capacitive Gate-Based Sensing* 29. January 2018 arXiv:1801.09759

[9] Ota, Takeshi Hayashi, Toshiaki Muraki, Koji Fujisawa, Toshimasa. Wide-band capacitance measurement on a semiconductor double quantum dot for studying tunneling dynamics. Applied Physics Letters. 96. 032104 - 032104. 10.1063/1.3285180. 2010.

[10] Bertram Brovang  Torbjørn Raasø Rasmussen *Simulation of quantom dot array* NBI, Københavns universitet https://github.com/BBTR/Bachelor/blob/master/Simulation.py

# 8 Appendix

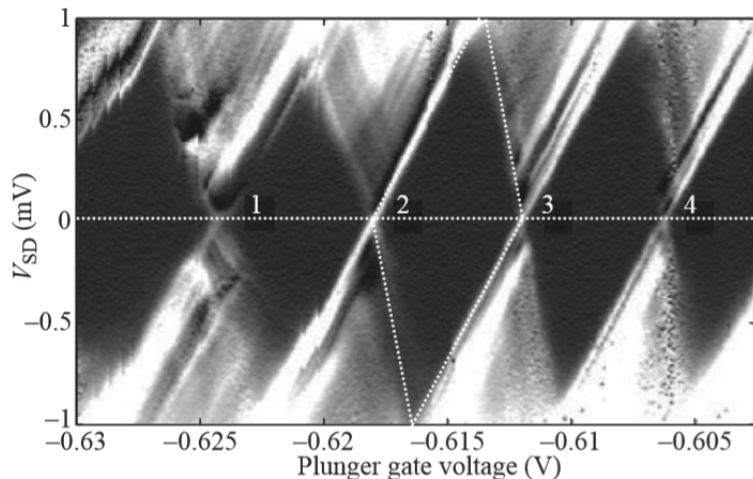## 8.1 Coulomb Diamonds

Coulomb Diamonds from [1]. Page: 343



Fig. 18.3 Coulomb blockade diamonds measured on a quantum dot realized on a parabolic quantum well. The grayscale represents the differential conductance $dI/dV_{SD}$ with zero encoded in black. Numbers 1–4 label zero source–drain voltage conductance peaks. One particular diamond is highlighted with a dotted boundary, the horizontal dotted line indicates $V_{SD} = 0$. (Reprinted with permission from Lindemann *et al.*, 2002. Copyright 2002 by the American Physical Society.)

Figure 30: Coulomb Diamonds [1]

## 8.2 How to set up the simulation

Following the Getting Started guide on qcodes github pages, we here present a quick guide to set you up with the required software and python packages to run the code. To setup the simulation from scratch on a new computer, install Anaconda, which is a platform that holds several different programming languages and gives a good overview of the packages installed for different editors. When you have done this open the Anaconda prompt and type in

conda env create -f environment.yml
activate qcodes
pip install qcodes

When this has been installed you will have an environment in your Anaconda navigator which is called qcodes. Open spyder with this environment and open the simulation. Run the entire script once and disable all import packages you can't load or install them as well. All packages that are nescesary for the simlutaion to run are in the qcodes environment.

## 8.3 How to use the simulation

When everything has been installed and is ready to go, you simply run the entire script once and then run the test function. You are now ready to take measurements. The first step is to run the entire script, which readies the capacitance matrix, with the gate to dot capacitances. It also readies the dot to dot capacitances, the functions that are used for the measurements and the functions that takes the measurements. The second step is to run the test function which initialises the dummy instruments, simtbpar and simtb01. The instrument simtbpar is our voltage supply and it has four gates, v1, v2, v3 and v4. All these gates can be set when taking measurements. When you call the simtb01, which is our multipurpose measurement device, it will know what the voltages are when taking for example the energy of the ground state. To take measurements use one of the function in the bottom half of the code.

## 8.4 Figures

## 8.5 List of figures

We've created many different figures and all of them with the parameters listed in this section. All capacitances are in aF. Capacitances:

**Symmetric triangle array**

$$c_1 = \begin{pmatrix} 3 & 1 & 1 & 1 & 0 & 0 & 0 & 0 \\ 1 & 3 & 1 & 1 & 0 & 0 & 0 & 0 \\ 1 & 1 & 3 & 1 & 0 & 0 & 0 & 0 \\ 1 & 1 & 1 & 3 & 0 & 0 & 0 & 0 \end{pmatrix} \tag{26}$$

For certain measurements this matrix was used with 5aF instead of 3aF for the dot to own gate coupling. c0102 ... c0304 = 1

The simulation processes this matrix such that only the active dots for each measurement will keep their capacitance, other unused dots are set to 0.

**Linear Triple dot** $c_1$ is still valid c0102 and c0203 = 1, others = 0

**Exctracted capacitances** for some measurements the extracted capacitances are used

$$c = \begin{pmatrix} 1.73 & 0.635 & 0.24 & 0.66 & 0 & 0 & 0 & 0 \\ 0.435 & 1.91 & 0.27 & X & 0 & 0 & 0 & 0 \\ 0.38 & 0.20 & 2.63 & X & 0 & 0 & 0 & 0 \\ 0.168 & X & X & 1.4 & 0 & 0 & 0 & 0 \end{pmatrix} \tag{27}$$

Here side and diag is used instead of the multiple different values for dot to dot capacitances. Here side is 1.05aF and diag is 0.75aF.

- Figure 2 Symmetric triangle array, measured with function spaghetti. No tunnel or reservoir coupling. 2 active dots.

- Figure 4 Extracted capacitances, measured with function CDsweep2d and no tunnel/reservoir coupling. 2 active dots.

- Figure 5a-c Extracted capacitances, measured with function ExpQCut and no tunnel/reservoir coupling. 2 active dots.

- Figure 6a-d Extracted capacitances, measured with function ExpQCut and tunnel/reservoir coupling of 4e-4. 2 active dots.

- Figure 7b Symmetric triangle array, measured with CDsweep2d and no tunnel/reservoir coupling. 1 active dot.

- Figure 10a-b Extracted capacitances, measured with Ediff and no tunnel/reservoir coupling.

- Figure 12 and 13 are measured with Symmetric triangle array with 5aF instead of 3aF, no tunnel/reservoir coupling, and measured with CDsweep2d. 3 active dots.

- Figure 14 same as 12/13 and measured with radialSearch3dSphere. 3 active dots.

- Figure 15a-h Symmetric Triangle array with no tunnel/reservoir coupling, measured with CDsweep2d and plotted using multiCDplot, plottype=3. 3 active dots.

- Figure 16 Extracted capacitances, no tunnel/reservoir broadening and measured with matrixsweep, plotted with CDplot, 3 active dots.

- Figure 17 Symmetric Triangle array with no tunnel/reservoir coupling, measured with matrixsweep and plotted with CDplot plottype=3, 3 active dots.

- Figure 18 and 19 Symmetric Triangle array, 2 active dots, tunnel and reservoir coupling of 4e-4, 1 of the capacitances is changed from 3aF to 3.001aF for the purpose of keeping the states identifiable after eigenvalue calculations. Measured with cut1d.

- Figure 20 and 21 Symmetric Triangle array, 2 active dots, tunnel/reservoir coupling of 4e-4 measured with expQCut.

- Figure 22 extracted capacitances, tunnel/reservoir coupling of 4e-4, 3 active dots, measured with expQ2Din3D.
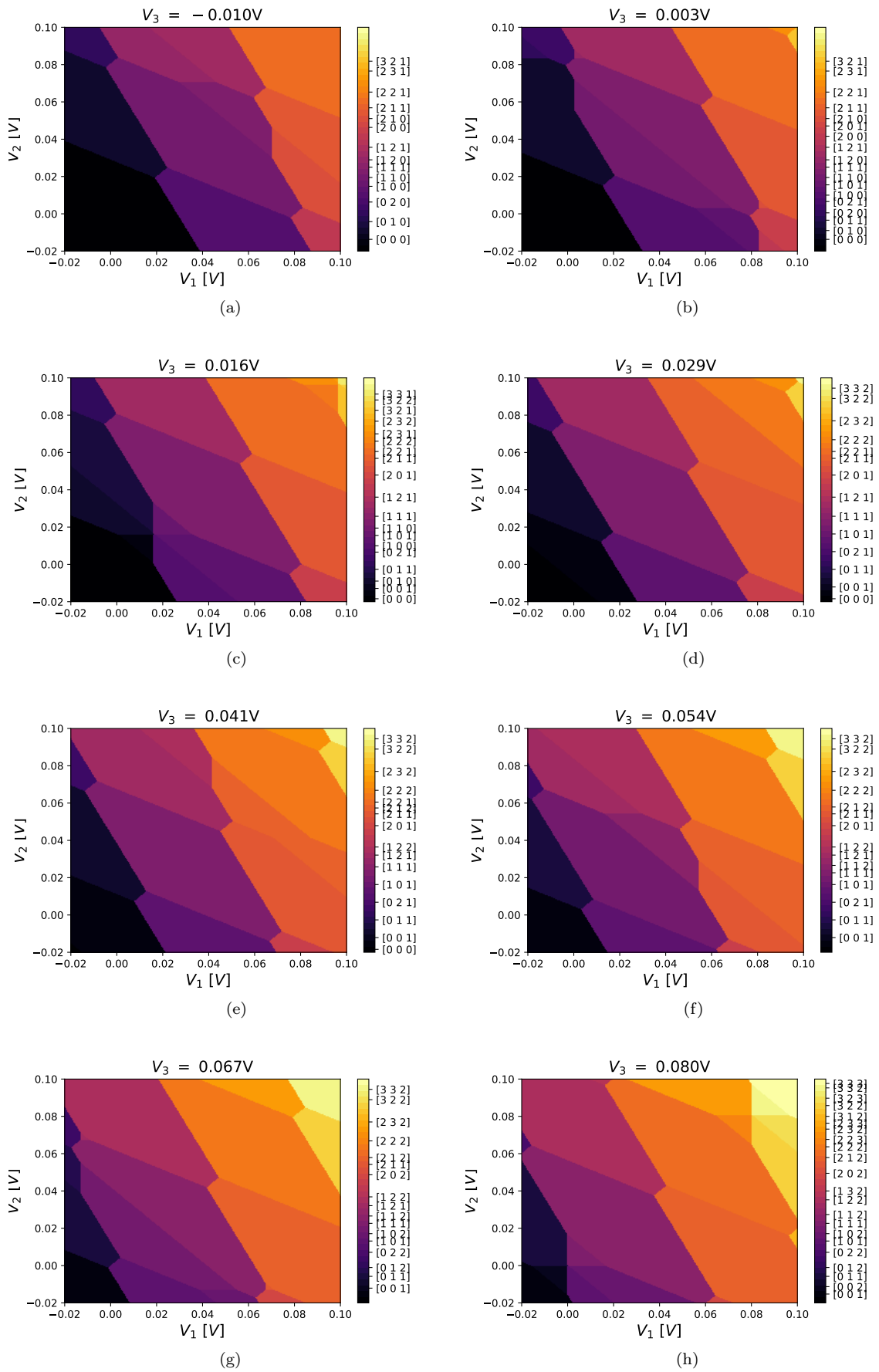
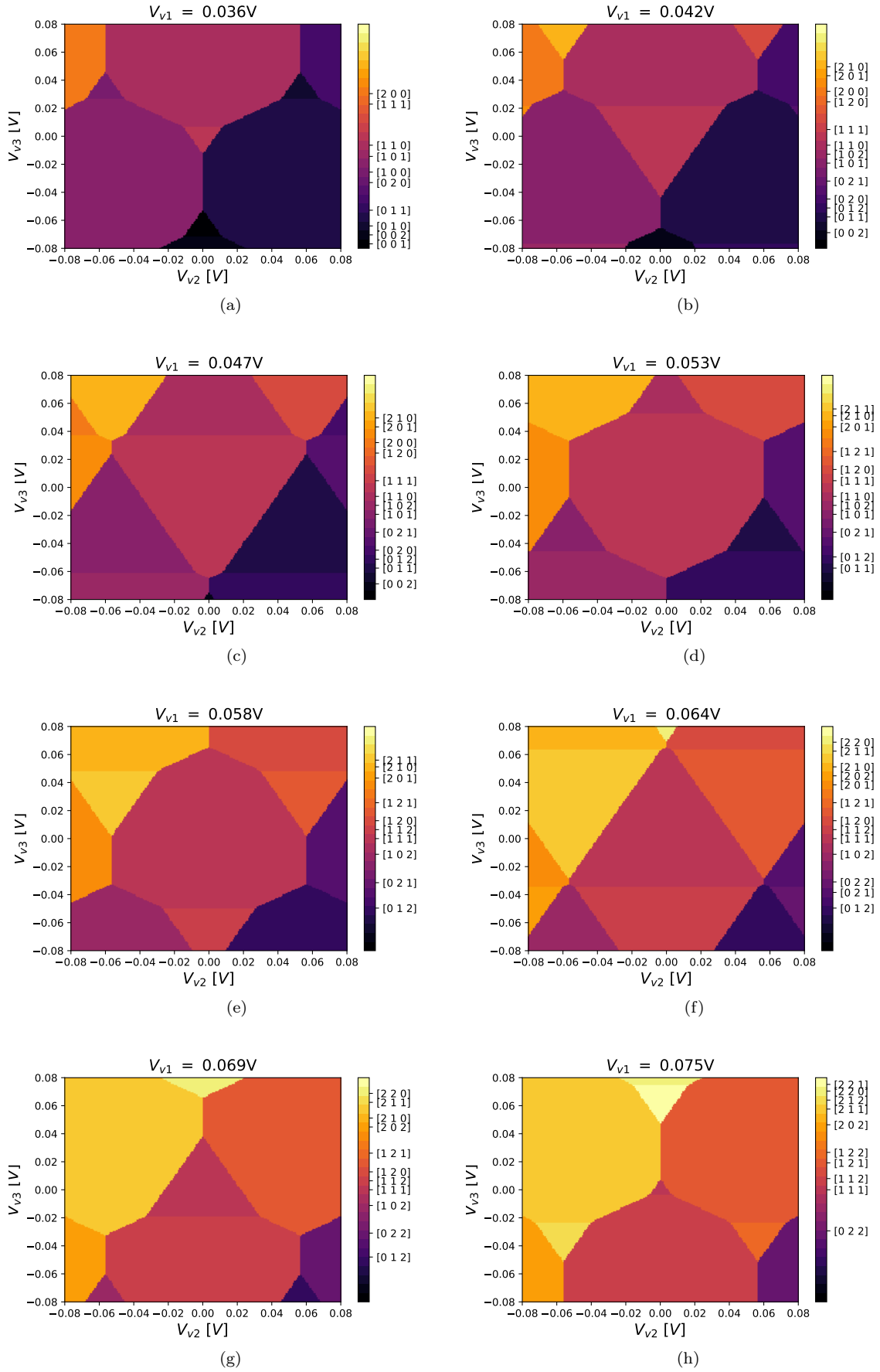Figure 31: Multiple Charge stability diagrams in native gate space containing the (111) region

Figure 32: Multiple Charge stability diagrams of virtual cuts perpendicular to the common mode, here in full colour